EUROPEAN HEMATOLOGY ASSOCIATION
haematologica
Journal of the European Hematology Association

Targeting the ER-mitochondria interface sensitizes leukemia cells towards cytostatics

by Fabian Koczian, Olga Nagło, Jan Vomacka, Binje Vick, Phil Servatius, Themistoklis Zisis, Britta Hettich, Uli Kazmaier, Stephan A Sieber, Irmela Jeremias, Stefan Zahler, and Simone Braig

Haematologica 2018 [Epub ahead of print]

Citation: Fabian Koczian, Olga Nagło, Jan Vomacka, Binje Vick, Phil Servatius, Themistoklis Zisis, Britta Hettich, Uli Kazmaier, Stephan A Sieber, Irmela Jeremias, Stefan Zahler, and Simone Braig. Targeting the ER-mitochondria interface sensitizes leukemia cells towards cytostatics. Haematologica. 2018; 103:xxx doi:10.3324/haematol.2018.197368

Targeting the ER-mitochondria interface sensitizes leukemia cells towards cytostatics

Fabian Koczian[1], Olga Nagło[1], Jan Vomacka[2], Binje Vick[3], Phil Servatius[4], Themistoklis Zisis[1], Britta Hettich[1], Uli Kazmaier[4], Stephan A. Sieber[2], Irmela Jeremias[3], Stefan Zahler[1], Simone Braig[1]

[1]Department of Pharmaceutical Biology, Ludwig Maximilian University of Munich, Munich, Germany.

[2]Department of Chemistry, Technical University of Munich, Garching, Germany.

[3]Research Unit Gene Vectors, Helmholtz Zentrum München, German Center for Environmental Health, Munich, Germany. [4]Institute of Organic Chemistry, Saarland University, Saarbrücken, Germany.

Corresponding author

Dr. Simone Braig, Department of Pharmacy, Butenandtstr. 5-13, 81377 Munich, Germany, Phone: 49-89-2180-77189, Fax: + 49-89-2180-77170, Email: simone.braig@cup.uni-muenchen.de

Conflict of Interest

The authors declare no conflict of interest.

Running title

PS89 - a novel option for combination therapy in acute leukemia

ABSTRACT

Combination chemotherapy has proved to be a favorable strategy to treat acute leukemia. However, the introduction of novel compounds remains challenging and is hindered by a lack of understanding their mechanistic interaction with established drugs. In the present study, we demonstrate a highly increased response of various acute leukemia cell lines, drug resistant cells and patient-derived xenograft cells by combining the recently introduced protein disulfide isomerase inhibitor PS89 with cytostatics. In leukemic cells, a proteomics based target fishing approach disclosed that PS89 impacts a whole network of endoplasmic reticulum homeostasis proteins. We elucidate that the strong apoptosis induction in combination with cytostatics is orchestrated by the PS89 target B-cell receptor-associated protein 31, which transduces apoptosis signals at the endoplasmic reticulum -mitochondria interface. Activation of caspase-8 and cleavage of BAP31 stimulate a pro-apoptotic crosstalk including endoplasmic reticulum calcium release and increased reactive oxygen species levels resulting in amplification of mitochondrial apoptosis. This study promotes PS89 as a novel chemosensitizing agent for acute leukemia treatment and uncovers that targeting the endoplasmic reticulum -mitochondria network of cell death is a promising approach in combination therapy.

INTRODUCTION

Despite the significant success in the management of childhood acute lymphoblastic leukemia (ALL) and acute myeloid leukemia (AML) with >80% and >60% survival respectively,(1) the outcome of relapsed or chemoresistant leukemia is still dismal.(2, 3) Especially in older patients, the balance of tolerable dosing versus effective cytotoxicity remains a major challenge. This issue is further exacerbated by the development of leukemic cell chemoresistances that have been demonstrated for several cytostatics including tubulin binders and topoisomerase inhibitors. (4, 5) In addition, the emergence of relapse-specific mutations of cancer cells are often associated with resistance towards thiopurines and glucocorticoids.(6, 7) Thus, novel pharmaceutical options are urgently needed for the improvement of current treatment regimens.

There is general consent that combination therapies benefit from the crosstalk of antileukemic agents, however the mechanisms of interaction have only been explored for a few.(8) Therefore, drug discovery is not only encouraged to identify novel compounds and targets, but also to enhance the

understanding of their interdependence with established cytostatics. The concept of network pharmacology has yielded high interest in recent years, especially regarding complex disease systems such as cancer.(8, 9) Following this principle, multi-target strategies rather than the 'one drug, one target' paradigm are proposed to be superior in rewiring cancer-specific networks and to overcome the system robustness of cancer cell phenotypes.(10, 11) Translating this concept to combinatorial drug treatment, a highly interesting issue is not only how networks are locally perturbed by individual compounds, but moreover how interventions at multiple cellular loci cooperate. Considering potential pro-apoptotic target networks, the crucial role of the ER-mitochondria 'social network of cell death' was recently stressed in several studies highlighting their dynamic interaction.(12, 13) In this context, the B-cell receptor-associated protein 31 (BAP31) was described as a substrate of caspase-8 and emerges as a communicator of apoptosis signals from the ER to mitochondria.(14, 15) Consistently, a role of the caspase-8-BAP31 axis has been demonstrated in ER stress triggered apoptosis of B-cell lymphocytic leukemia cells.(16) ER stress results from an imbalance between ER protein load and folding capacity. Protein disulfide isomerases (PDIs) represent a crucial family of enzymes to maintain oxidative protein folding and ER homeostasis.(17) Hence, these proteins have been recognized as exciting novel targets in cancer research.(18) Furthermore, overexpression of PDIs has been discovered in leukemia and linked to chemoresistance.(19-21)

Recently, we introduced the first reversible small-molecule PDI inhibitor PS89 which binds in close proximity to the catalytic centers of PDI.(22) Moreover and contrary to other PDI inhibitors that feature severe cytotoxicity,(23, 24) PS89 is not toxic up to micromolar concentrations, though it has been shown to highly enhance etoposide-induced apoptosis. This exceptional character of effective chemosensitization at subtoxic doses motivated not only further combination therapy studies with PS89, but also a deeper analysis of its interactive signaling. In the present work, PS89 is set on stage as a novel therapeutic option for acute leukemia treatment. The favorable attributes of PS89 and its broad applicability are highlighted in ALL and AML cell lines, drug resistant cells as well as patient-derived xenograft (PDX) cells. Hence, the critical networks integrated in the synergistic pro-apoptotic signaling of PS89 in combination with cytostatics were identified, thus emphasizing the crucial function of ER-mitochondria communication for successful combination therapies.

METHODS

Cell culture

Jurkat cells (WT, CASP8 deficient, Bcl-2 and Bcl-xL overexpressing) were kindly provided by P. H. Krammer (Heidelberg, Germany). CCRF-CEM and vincristine resistant (VCR-R) CEM (25, 26) were obtained from M. Kavallaris (Sydney, Australia), HEK 293 and Hela cells from DSMZ (Braunschweig, Germany) and HL-60 from ATCC (Manassas, VA, USA). All cell lines were maintained in ATCC recommended culture conditions.

PDX cells, PBMCs and CD34 positive cells

The model of ALL and AML patients' leukemia cells growing in mice has been described previously.(27, 28) Ethical statements and approvals are outlined in SI. In the present study, patient-derived xenograft (PDX) cells were freshly isolated from the bone marrow or spleen of NSG mice and cultivated in presence or absence of compounds. Peripheral blood mononuclear cells (PBMCs) were freshly isolated from EDTA-anticoagulated blood of healthy donors by gradient centrifugation using Ficoll-Paque PLUS (GE Healthcare, Chicago, IL, USA) according to manufacturer's instructions. PBMCs were maintained in RPMI 1640 with 2 mM glutamine supplemented with 20% (v/v) FCS and 1 mM pyruvate. CD34 positive cells were identified by staining with FITC conjugated anti-human CD34 antibody (BD Biosciences, Heidelberg, Germany) as described by the manufacturer and analyzed by Flow Cytometry as described in (29).

Ethical statements

Written informed consent was obtained from all patients or legal guardians in the cases where patients were minors. The study was performed in accordance with the ethical standards of the responsible committee on human experimentation (written approval by the ethics committee of the University Hospital of the LMU Munich, number 068-08) and with the Helsinki Declaration of 1975, as revised in 2000. All animal trials were performed in accordance with the current ethical standards of the official committee on animal experimentation (written approval by Regierung von Oberbayern, number 55.2-1-54-2532-95-10).

Activity-based protein profiling (ABPP)

Jurkat cells were incubated with unmodified PS89 (100 µM) or DMSO as control for 45 min at 37°C and in a second step with the PS89 photo probe (20 µM) or DMSO as control for 45 min at 37°C. Cells were lysed in 1 ml PBS with 1% (v/v) NP40 and 1% (w/v) sodium deoxycholate and sonication for 15 sec on ice. Sample preparation and mass spectrometry analysis of target proteins by gel-free ABPP and dimethyl labeling was performed as previously described.(30) Cutoff criteria for target identification: (1) enrichment by photo probe $\log_2$ Probe/DMSO >1.6, $-\log_{10}$ p-value >2 and (2) PS89 competition $\log_2$ Probe/PS89 >0. Data shown contain the results of n=3 biological replicates.

Details of the methods used are available in the *Online Supplementary Appendix.*

RESULTS

PS89 sensitizes acute leukemia cell lines and PDX cells towards cytostatics

The concept of chemosensitization with the recently introduced protein disulfide isomerase (PDI) inhibitor PS89 was initially evaluated in a dose-response apoptosis assay. While PS89 was applied at a fixed subtoxic dose, the concentration of etoposide (ETO) could be reduced at least by half to achieve equal cytotoxicity applying the combination treatment. This is in line with a shifted EC_{50} value by more than 2-fold (Figure 1a, Bliss values indicating synergistic effects of PS89 in combination with etoposide are shown in Supplementary table S1a). Whereas etoposide treated cells showed a pronounced G2 arrest, PS89 had no effect on the cell cycle (Supplementary Figure S1a). Further, PS89 combination treatments with subtoxic etoposide concentrations synergistically inhibited Jurkat cell proliferation and colony formation (Supplementary Figure S1b+c). The ability of PS89 to induce synergistic apoptosis with diverse cytostatics could be translated to acute leukemia cells of different lineages. This was demonstrated by PS89 combinations both with daunorubicin (DNR) in HL-60 and vincristine (VCR) in CCRF-CEM cells (Figure 1b, synergism calculations according to Bliss independence model are shown in supplementary table S1b) as well as in combination with 6-Mercaptopurine (6-MP) or Dexamethasone (DEX), respectively, in Jurkat and HL-60 cells (Supplementary Figures S1d-f). Further, vincristine resistant (VCR-R) CEM cells show high apoptosis

rates towards 100 nM vincristine in combination with PS89 (38.3% apoptotic cells), while being resistant towards 10-fold higher vincristine concentrations without co-stimulation (1000 nM VCR 6.8% apoptotic cells, Figure 1b). Moreover, clonogenic growth of vincristine-resistant CEM and HL-60 cells is significantly abrogated upon treatment with PS89 in combination with vincristine or 6-mercaptopurine, respectively (Supplementary Figure S1g and h). In PS89 combination treatments of Jurkat, VCR-R CEM, CCRF-CEM and HL-60 cells with etoposide, vincristine or 6-mercaptopurine, respectively, activation of caspase-3 and PARP cleavage indicate a clear induction of apoptotic cell death (Figure 1c, Supplementary Figure S2). In addition, apoptosis was prevented by the pan-caspase inhibitor QVD-OPh (Supplementary Figure S3). Since pharmacokinetic studies demonstrated that PS89 has a very short half-life in blood serum (data not shown), in vivo experiments at not feasible at the moment. However, the broad applicability of PS89 as chemosensitizing agent was confirmed in ALL and AML patient-derived xenograft (PDX) cells of diverse background (Supplementary Table S2). PDX samples treated with PS89 and vincristine (Figure 1d) or PS89 and daunorubicin (Figure 1e), respectively, showed clearly increased apoptosis rates after combination treatment compared to single cytostatics (distinct p-values are presented in Supplementary table S3a and b). Bliss independence model confirms a synergistic effect of vincristine or daunorubicin, respectively, in combination with PS89 in ALL and AML patient derived xenografts cells. Yet, PS89 was non-toxic which is in accordance with previous results. Notably, low response towards the combination treatments was observed in healthy peripheral blood mononuclear cells (PBMCs) as well as CD34 positive hematopoietic stem cells compared to ALL and AML patient samples (Figure 1d,e and f, Supplementary tables S3).

Proteomics identifies a PS89 target network affecting ER homeostasis

To elucidate the impressive pro-apoptotic mechanisms behind PS89 combination treatments, the role of the prominent PS89 target protein disulfide isomerase (PDI) was studied by genetic knockdown and overexpression experiments. Since neither silencing of PDI mimicked nor overexpression of PDI rescued the sensitizing effect of PS89 on apoptosis induction or inhibition on proliferation (Figure 2a and Supplementary Figure S4), we assumed that PS89 addresses additional cellular structures. In order to identify the proposed multi-target characteristics of PS89, activity-based protein profiling (ABPP) was performed in Jurkat cells as depicted in Figure 2b. The PS89 photo probe modified by an alkyne handle (structure shown in Figure 2b) was covalently linked to cellular targets in presence or

absence of PS89. Co-incubation with the unmodified compound acting as a competitor was performed to exclude the identification of targets that were only enriched by the probe, but not by PS89. Including both data sets as well as their reproducibility expressed as p-values (cutoff criteria as described in materials and methods), a total of 42 target proteins were identified (Figure 2c and Supplementary Table S4). Performing protein-protein interaction analysis using the STRING database(31), 23 out of 42 PS89 target proteins were involved in a protein interaction network (Figure 2d). This was further analyzed by Gene Ontology (GO) functional classification for common cellular components and biological processes.(32) A highly significant number of PS89 target proteins was assigned to be located in the endoplasmic reticulum (FDR 5.9e-12) and described to be involved in cellular homeostasis, in particular cell redox homeostasis (FDR 9.1e-07 and 6.7e-09, Figure 2d+e). Thereby, B-cell receptor-associated protein 31 (BAP31), which is described to be involved in ER stress mediated apoptosis signaling pathways,(15) was identified as one of the most prominent target proteins (Figure 2c and Supplementary Table S4).

Apoptosis induced by PS89 combination treatments is mediated via the BAP31-caspase-8 axis

To validate BAP31 as direct target of PS89, a co-staining was performed using a BAP31-specific antibody and the photo probe linked to a rhodamine reporter dye by click chemistry. Besides the supposed ER specificity, overlapping fluorescence revealed distinct co-localized ER network structures of PS89 photo probe-rhodamine (red) and BAP31-Alexa 488 (green, Figure 3a). No background staining of either the rhodamine-azide or the Alexa 488 secondary antibody was detected (Supplementary Figure S5). In addition, direct binding of PS89 photo probe to BAP31 was further evaluated by single-point fluorescence correlation spectroscopy (FCS) measurements. Here, random motion of fluorescent molecules into and out of a stationary laser focus results in fluctuations in fluorescence intensity, which can be monitored by confocal laser scanning microscopy. Hence, diffusion and concentration values of the PS89 photo probe +/- different amounts of recombinant BAP31 protein can be calculated by fitting of the autocorrelation curves (Fig. 3b, Supplementary Figure S6). As shown in Fig 3b and S6, whereas the PS89 photo probe alone has a distinct diffusion value of ~274 $\mu m^2/s$, two diffusing components were detected in presence of recombinant BAP31 protein (D2 and D1). The fast diffusing species D2 characterizes remaining unbound photo probe (showing a diffusion value of ~264 $\mu m^2/s$), whereas the slowly diffusing part D1 describes the PS89 bound to BAP31. This decrease of PS89 diffusion after addition of the BAP31 protein indicates a

strong direct interaction between the two and the resulting diffusion value of ~70 $\mu m^2/s$ is in agreement with literature values for proteins of that size (33). Of note, no significant change in concentration was observed after addition of the protein in the solution (Supplementary Figure S6d).

As the BAP31 protein complex has been shown to serve as a platform for caspase-8 activation upon apoptotic stimuli,(14) the influence of PS89 on caspase-8 activation after etoposide treatment was examined. Whereas stimulation with etoposide and PS89 alone has only modest effects on caspase-8 cleavage, combination of both compounds results in strong activation of caspase-8 in Jurkat, CCRF-CEM as well as ALL PDX patient samples (Figure 3c, Supplementary Figure S7a+b). Moreover, cleavage of BAP31 into the pro-apoptotic p20BAP31 fragment or decreased expression of BAP31 proform, respectively, was only present in PS89 combination treated Jurkat, CCRF-CEM and ALL PDX cells and, as an early trigger, already detectable after 24 h (Figure 3b, Supplementary Figure S7). Treatment-independent interaction of procaspase-8 with BAP31 could be demonstrated by co-immunoprecipitation (Figure 3d). Interestingly, binding of cleaved p43/p41 caspase-8 to BAP31 was only detected in the presence of both stimulants, PS89 and etoposide (Figure 3d, for normalization to BAP31 see supplementary Figure S8). In order to investigate whether apoptosis induction by PS89 and etoposide combination is critically dependent on caspase-8 activity, cells were stimulated in presence of the specific and irreversible caspase-8 inhibitor Z-IETD-FMK. As shown in Figure 3e, inhibiting the activity of caspase-8 results in diminished apoptosis upon treatment with etoposide and PS89. In accordance, the ratio of apoptotic cells in PS89 combination vs. etoposide single treated cells is reduced in caspase-8 deficient Jurkat compared to wildtype cells (1.7-fold in CASP8 -/- vs. 2.8-fold in WT Jurkat, Supplementary Figure S9). Next, we examined the functional effects of impairing the expression of the direct PS89 target BAP31 by siRNA. Whereas PS89 significantly enhanced etoposide triggered apoptosis in control cells, no synergistic effect on apoptosis induction upon treatment with PS89 and etoposide could be detected in siBAP31 transfected cells (Figure 3f).

ER and mitochondrial stress triggers are amplified by PS89

To investigate the consequences of PS89 and etoposide at the ER-mitochondria interface, calcium release from the ER to the cytosol was evaluated by FACS analysis. A shifted Cal-520 fluorescence intensity and thus higher levels of cytosolic calcium was observed in PS89 combination treated Jurkat, CCRF-CEM and HL-60 and ALL PDX cells compared to etoposide single treatment (Figure 4a, Supplementary Figure S10). Interestingly, amplification of calcium release was observed from 24 h to

48 h in PS89 combination, but neither in etoposide, daunorubicin nor vincristine single treated cells. Loss of mitochondrial membrane integrity analyzed by JC-1 staining was increased by co-incubation of etoposide with PS89 (Figure 4b) resulting in release of cytochrome c into the cytosol (Figure 4c, Supplementary Figure S11) and elevated levels of reactive oxygen species (ROS) in Jurkat, CCRF-CEM and HL-60 cells (Figure 4d, Supplementary Figure S12). ROS signaling from mitochondria to the ER provokes further disturbance of ER redox homeostasis and finally closes the feedback loop.

The eminent role of functional mitochondrial apoptosis signaling was reinforced studying stable leukemia cells overexpressing the antiapoptotic proteins Bcl-2 and Bcl-xL. Interestingly, these clones showed a significantly lower sensitivity towards PS89 in combination with etoposide than the empty vector cell line Jurkat*/neo* (Figure 4e). Moreover, the specific targeting of mitochondria with the Bcl-2 inhibitor ABT-199 resulted in synergistic apoptosis in combination with PS89 (Figure 4f, Bliss values are shown in Supplementary Table S5), thus substantiating the importance of cytostatics-induced mitochondrial damage provoking the chemosensitizing effect of PS89.

The ER-mitochondria interface mediates mutual amplification of PS89 and cytostatics triggered apoptosis

In summary, PS89 strongly increases mitochondrial apoptosis through a crosstalk and mutual amplification of pro-apoptotic stress signals triggered by cytostatics (Figure 5). The polypharmacological profile of PS89 affecting a network of ER homeostasis proteins is represented by its main targets PDI and BAP31. Upon apoptotic stimuli of cytostatics and exclusively in presence of PS89, BAP31 is cleaved by caspase-8 to pro-apoptotic p20BAP31. Calcium release from the ER and increased ER stress promote loss of mitochondrial membrane potential ($\Delta\Psi m$) and apoptosis. In turn, elevated production of reactive oxygen species (ROS) feeds back to the ER and provokes further ER stress and calcium release. The mutual amplification of ER-mitochondrial stress triggers finally leads to synergistic activation of caspases and apoptosis.

DISCUSSION

In the present study, we demonstrate that activating the apoptotic machinery at the ER-mitochondria interface is a highly promising approach for combinatory drug treatment. Co-stimulation of cytostatics with subtoxic doses of the novel PDI inhibitor PS89 resulted in a highly synergistic apoptosis response in a broad range of ALL and AML cell lines and human xenograft cells derived from initial diagnosed and relapsed patients. In order to exploit this successful strategy, our work in particular sheds light on the intriguing question how a drug at non-toxic concentrations could become highly effective in combination with cytostatics.

The small molecule PS89 was previously identified as a potent chemosensitizing agent, which inhibits protein disulfide isomerase (PDI).(22) Notably, although PDI plays a key role in maintenance of oxidative protein folding in the ER, no induction of ER stress or unfolded protein response was observed by applying PS89 alone, but only in combination with etoposide. This indicated that activation of the ER stress response results from the disability of the ER to resolve a stress condition which is provoked in cooperation with cytostatics.(22)

As it is known that many cytostatics induce cell death via activation of the mitochondrial apoptosis pathway(34) and moreover, an increasing number of studies indicate a pivotal role of ER-mitochondria communication for cell fate decision (reviewed in (35-37)), we investigated a potential PS89 triggered crosstalk between ER stress and mitochondrial damage. Activity-based protein profiling (ABPP) conducted in Jurkat ALL cells identified that next to PDI, PS89 targets a network of proteins located at the ER, among those B-cell receptor-associated protein 31 (BAP31). Interestingly, it is described that etoposide stimulates caspase-8 mediated cleavage of BAP31 to pro-apoptotic p20BAP31 at the ER-mitochondria interface, which results in calcium release from the ER and induction of mitochondrial apoptosis.(14) Moreover, under ER stress conditions, BAP31 interacts with cell death-inducing p53-target protein 1 (CDIP1) leading to cleavage of BAP31, recruitment of Bcl-2 and mitochondrial apoptosis via Bax oligomerization.(15) Therefore, we presumed that by inhibiting PDI and further ER stress related proteins in addition to directly targeting BAP31, PS89 tunes pro-apoptotic feedback from the ER to mitochondria, which results in amplification of cell death signaling in combination therapy.

To confirm the central role of the caspase-8-BAP31 axis in PS89 combination treatment, the processing and activation of the respective proteins was investigated. Indeed, BAP31 cleavage in co-stimulated cells could be observed already after early time points. Interestingly, we could show for the

first time the intermediate p43/41 cleavage product of caspase-8 associated with BAP31, which still holds a death effector domain. This supports the suggestion that further processing into the finally active p18 fragment in fact happens at the BAP31 complex.(14) As we detected p43/41 caspase-8 association as well as BAP31 cleavage only in PS89 combination treated cells and silencing of BAP31 rescued the chemosensitizing effect of PS89, we conclude that BAP31 binding is a crucial feature of PS89 to mediate an efficient ER-mitochondria communication. Subsequently, an amplification of calcium release was shown in PS89 combination, but not in etoposide single treated cells. Mitochondria-directed calcium flux finally promotes mitochondrial outer membrane permeabilization (MOMP), ROS accumulation and cytochrome c release(13, 36) which was demonstrated to be increased in PS89 co-stimulated cells as well. Hence, PS89 is able to augment apoptotic triggers of cytostatics by interfering with the ER-mitochondria feedback loop. Noteworthy, cells stably overexpressing anti-apoptotic mitochondrial proteins Bcl-2 und Bcl-xL, respectively, are less sensitive towards the combination treatment, presumably due to an impaired mitochondrial apoptosis machinery. With reference to the concept of the ER-mitochondria 'social network of cell death',(13) it is conceivable that the ER-mitochondrial feedback loop procures the crucial pro-apoptotic amplification effect by compromising numerous mitochondria, even if the original stimulus targeted only a few.

In order to further comprehend how stress triggers are communicated from mitochondria to the ER and back, future prospects of the mediator BAP31 require a closer examination of the BAP31 complex. As shown in previous studies, Fis1 bridges mitochondria and ER-located BAP31 which seems to be further under control of ER stress inducible CDIP1 as well as anti-apoptotic Bcl-2 and Bcl-xL.(14, 15) However, the dynamics regulating the balance of pro- and anti-apoptotic proteins within the complex have not been clarified yet. As PS89 is to our knowledge the first BAP31 binding small-molecule compound, which facilitates BAP31 cleavage, it might serve as a valuable tool not only to study the dynamics of the BAP31 protein complex and manipulate decisive BAP31 interactions that favor the pro-apoptotic output, but also to enable in-depth characterization of BAP31 as a prospective pharmacological addressable target protein in different diseases. Referring to hematological malignancies, this is further encouraged by the finding that overexpression of BAP31 seems to correlate with chemoresistance as shown in fludarabine-resistant mantle cell lymphoma (38) as well as proteasome inhibitor-adapted myeloma cells.(39)

In terms of prospective anti-cancer therapies, targeting pro-apoptotic ER-mitochondria crosstalk by combinatory pharmaceutical intervention offers versatile options. For example, BH3 mimetics are a

valuable novel compound class to trigger intrinsic apoptosis and encouraging results were recently shown in an AML phase II trial with ABT-199.(40) As shown here, ABT-199 in combination with PS89 strongly increases cell death in Jurkat cells compared to single treated cells. This further underlines the concept of amplification by communication between ER and mitochondria as a promising strategy to develop new drugs able to trigger apoptosis and overcome therapy resistance. Moreover, next to PDI targeting agents, proteasome or HSP90 inhibitors might be highly promising candidates for combination with mitochondria damaging substances to tune pro-apoptotic ER stress response.(41)

In conclusion and response to the question how PS89 is able to sensitize acute leukemia cells, the ER-mitochondria interface was identified as the key platform in the pro-apoptotic signaling cascades mediating the cytotoxic effects of PS89 in combination with cytostatics. By directly affecting PDI and BAP31, PS89 mutually amplifies ER and mitochondrial stress triggers, resulting in strong chemosensitizing effects. Hence, this study discloses the potential of targeting the ER-mitochondria apoptosis network as a novel and encouraging strategy in anti-cancer therapy.

ACKNOWLEDGEMENTS

We thank Judith Hoffmann for the supply of PS89 and the photo probe, and Kerstin Loske as well as Silvia Schnegg for technical assistance. The project was financially supported by the Dr. Robert Pfleger foundation.

REFERENCES

1. Ward E, DeSantis C, Robbins A, et al. Childhood and adolescent cancer statistics, 2014. CA Cancer J Clin. 2014;64(2):83-103.

2. Pui C-H, Robison LL, Look AT. Acute lymphoblastic leukaemia. Lancet. 2008;371(9617):1030-1043.

3. Döhner H, Weisdorf DJ, Bloomfield CD. Acute myeloid leukemia. New Engl J Med. 2015;373(12):1136-1152.

4. Kavallaris M. Microtubules and resistance to tubulin-binding agents. Nat Rev Cancer. 2010;10(3):194-204.

5. Nitiss JL. Targeting DNA topoisomerase II in cancer chemotherapy. Nat Rev Cancer. 2009;9(5):338-350.

6. Dieck CL, Tzoneva G, Forouhar F, et al. Structure and Mechanisms of NT5C2 Mutations Driving Thiopurine Resistance in Relapsed Lymphoblastic Leukemia. Cancer Cell. 2018;34(1):136-147.e6.

7. Nicholson L, Evans CA, Matheson E, et al. Quantitative proteomic analysis reveals maturation as a mechanism underlying glucocorticoid resistance in B lineage ALL and re-sensitization by JNK inhibition. Br J Haematol. 2015;171(4):595-605.

8. Jia J, Zhu F, Ma X, et al. Mechanisms of drug combinations: interaction and network perspectives. Nat Rev Drug Discov. 2009;8(2):111-128.

9. Barabási A-L, Gulbahce N, Loscalzo J. Network medicine: a network-based approach to human disease. Nat Rev Genet. 2011;12(1):56-68.

10. Zimmermann GR, Lehar J, Keith CT. Multi-target therapeutics: when the whole is greater than the sum of the parts. Drug Discov Today. 2007;12(1):34-42.

11. Hopkins AL. Network pharmacology: the next paradigm in drug discovery. Nat Chem Biol. 2008;4(11):682-690.

12. Eletto D, Chevet E, Argon Y, et al. Redox controls UPR to control redox. J Cell Sci. 2014;127(17):3649-3658.

13. Grimm S. The ER–mitochondria interface: The social network of cell death. Biochim Biophys Acta. 2012;1823(2):327-334.

14. Iwasawa R, Mahul-Mellier AL, Datler C, et al. Fis1 and Bap31 bridge the mitochondria–ER interface to establish a platform for apoptosis induction. EMBO J. 2011;30(3):556-568.

15. Namba T, Tian F, Chu K, et al. CDIP1-BAP31 complex transduces apoptotic signals from endoplasmic reticulum to mitochondria under endoplasmic reticulum stress. Cell Rep. 2013;5(2):331-339.

16. Rosati E, Sabatini R, Rampino G, et al. Novel targets for endoplasmic reticulum stress-induced apoptosis in B-CLL. Blood. 2010;116(15):2713-2723.

17. Galligan JJ, Petersen DR. The human protein disulfide isomerase gene family. Hum Genomics. 2012;6:6.

18. Xu S, Sankar S, Neamati N. Protein disulfide isomerase: a promising target for cancer therapy. Drug Discov Today. 2014;19(3):222-240.

19. Haefliger S, Klebig C, Schaubitzer K, et al. Protein disulfide isomerase blocks CEBPA translation and is up-regulated during the unfolded protein response in AML. Blood. 2011;117(22):5931-5940.

20. Higa A, Taouji S, Lhomond S, et al. Endoplasmic Reticulum Stress-Activated Transcription Factor ATF6α Requires the Disulfide Isomerase PDIA5 To Modulate Chemoresistance. Mol Cell Biol. 2014;34(10):1839-1849.

21. Trivedi R, Müller G, Rathore M, et al. Anti-Leukemic Activity of Shikonin: Role of ERP57 in Shikonin Induced Apoptosis in Acute Myeloid Leukemia. Cell Physiol Biochem. 2016;39(2):604-616.

22. Eirich J, Braig S, Schyschka L, et al. A small molecule inhibits protein disulfide isomerase and triggers the chemosensitization of cancer cells. Angew Chem Int ED Engl. 2014;53(47):12960-12965.

23. Xu S, Butkevich AN, Yamada R, et al. Discovery of an orally active small-molecule irreversible inhibitor of protein disulfide isomerase for ovarian cancer treatment. Proc Natl Acad Sci USA. 2012;109(40):16348-16353.

24. Vatolin S, Phillips JG, Jha BK, et al. Novel Protein Disulfide Isomerase Inhibitor with Anticancer Activity in Multiple Myeloma. Cancer Res. 2016;76(11):3340-3350.

25. Haber M, Norris MD, Kavallaris M, et al. Atypical Multidrug Resistance in a Therapy-induced Drug-resistant Human Leukemia Cell Line (LALW-2): Resistance to Vinca Alkaloids Independent of P-Glycoprotein. Cancer Res. 1989;49(19):5281-5287.

26. Verrills NM, Walsh BJ, Cobon GS, et al. Proteome Analysis of Vinca Alkaloid Response and Resistance in Acute Lymphoblastic Leukemia Reveals Novel Cytoskeletal Alterations. J Biol Chem. 2003;278(46):45082-45093.

27. Terziyska N, Alves CC, Groiss V, et al. In Vivo Imaging Enables High Resolution Preclinical Trials on Patients' Leukemia Cells Growing in Mice. PLoS One. 2012;7(12):e52798.

28. Vick B, Rothenberg M, Sandhöfer N, et al. An advanced preclinical mouse model for acute myeloid leukemia using patients' cells of various genetic subgroups and in vivo bioluminescence imaging. PLoS One. 2015;10(3):e0120925.

29. Fukuda J, Kaneko T, Egashira M, et al. Direct measurement of CD34+ blood stem cell absolute counts by flow cytometry. Stem Cells. 1998;16(4):294-300.

30. Vomacka J, Korotkov VS, Bauer B, et al. An Aromatic Hydroxyamide Attenuates Multiresistant Staphylococcus aureus Toxin Expression. Chemistry. 2016;22(5):1622-1630.

31. Szklarczyk D, Franceschini A, Wyder S, et al. STRING v10: protein–protein interaction networks, integrated over the tree of life. Nucleic Acids Res. 2015;43(Database issue):D447-452.

32. Consortium GO. Gene ontology consortium: going forward. Nucleic Acids Res. 2015;43(Database issue):D1049-D1056.

33. Krouglova T, Vercammen J, Engelborghs Y. Correct diffusion coefficients of proteins in fluorescence correlation spectroscopy. Application to tubulin oligomers induced by Mg2+ and Paclitaxel. Biophys J. 2004;87(4):2635-2646.

34. Chonghaile TN, Sarosiek KA, Vo T-T, et al. Pretreatment mitochondrial priming correlates with clinical response to cytotoxic chemotherapy. Science. 2011;334(6059):1129-1133.

35. Bhat TA, Chaudhary AK, Kumar S, et al. Endoplasmic reticulum-mediated unfolded protein response and mitochondrial apoptosis in cancer. Biochim Biophys Acta Rev Cancer. 2017;1867(1):58-66.

36. Shore GC, Papa FR, Oakes SA. Signaling cell death from the endoplasmic reticulum stress response. Curr Opin Cell Biol. 2011;23(2):143-149.

37. Simmen T, Herrera-Cruz MS. Cancer: Untethering Mitochondria from the ER? Front Oncol. 2017;7:105.

38. Lorkova L, Scigelova M, Arrey TN, et al. Detailed functional and proteomic characterization of fludarabine resistance in mantle cell lymphoma cells. PLoS One. 2015;10(8):e0135314.

39. Soriano G, Besse L, Li N, et al. Proteasome inhibitor-adapted myeloma cells are largely independent from proteasome activity and show complex proteomic changes, in particular in redox and energy metabolism. Leukemia. 2016;30(11):2198-2207.

40. Konopleva M, Pollyea DA, Potluri J, et al. A phase 2 study of ABT-199 (GDC-0199) in patients with acute myelogenous leukemia (AML). Blood. 2014;124(21):118.

41. Wang M, Kaufman RJ. The impact of the endoplasmic reticulum protein-folding environment on cancer development. Nat Rev Cancer. 2014;14(9):581-597.

FIGURE LEGENDS

Figure 1. Chemosensitization of acute leukemia cells with PS89. (**a** and **b**) Apoptosis of Jurkat, HL-60, CCRF-CEM and vincristine resistant (VCR-R) CEM cells treated with cytostatics (ETO: etoposide, VCR: vincristine, DNR: daunorubicin) in presence or absence of 25 µM PS89. Percentage of apoptotic cells was determined by FACS analysis after 48 h. (**c**) Jurkat and VCR-R CEM were cultured for 48 h in drug supplemented medium and apoptosis was analyzed by immunoblotting. (**d** and **e**) Freshly isolated PBMCs and ALL or AML PDX cells were treated with PS89 and cytostatics for 48 h or 72 h, respectively. Apoptotic cells were determined by FACS analysis and specific apoptosis was calculated towards untreated controls. Synergism was calculated using Bliss independence model. **(f)** PBMCs were treated for 48h with indicated drugs. CD34 positive cells were identified by flow cytometry using a FITC conjugated CD34 antibody. Cell death was analyzed by propidium iodide staining.

Figure 2. Analysis of PS89 target proteins. (**a**) PDI genetically modified Jurkat cells (siRNA silencing, 48 h) or HEK cells (PDI overexpression, 24 h) were treated with etoposide (ETO) and / or PS89 for 48 h and 72 h, respectively. Apoptosis was determined by FACS analysis and inhibition of proliferation by CellTiter-Blue staining. PDI expression was analyzed by immunoblotting, actin was used as loading control. (**b**) Principle of activity-based protein profiling (ABPP) with the PS89 photo probe covalently linked to its cellular targets (adapted from Vomacka *et al* (30)). (**c**) Volcano plot of target proteins enriched by the PS89 photo probe vs. DMSO (left). Targets with >3-fold enrichment ($\log_2$ Probe / DMSO >1.6) and $-\log_{10}$ p-value >2 are highlighted. Ranking of targets according to the degree of competition by unmodified PS89 (right). (**d** and **e**) Target network analysis of n=42 most enriched PS89 binding proteins with STRING v10. Proteins involved in the most prominent Gene Ontology classes are highlighted (Cellular Component - orange circles; Biological Process - green dots).

Figure 3. Signal transduction via the BAP31-caspase-8 axis. (**a**) Immunofluorescence staining of BAP31 (green) and localization of the PS89 photo probe linked to a rhodamine reporter (red) in Hela cells. Representative original images (upper row) and areas of co-localization analyzed with Leica LAS X software (bottom row) are shown. (**b**) Diffusion values of PS89 and PS89+BAP31 showing an interaction between probe and protein. Control sample of 50 nM freely diffusing PS89 in buffer solution

and 50nM PS89 probe plus 50nM BAP31 protein in buffer solution were analyzed by single-point FCS measurements. The diffusion coefficient of the probe alone was measured after 1 species fitting of the autocorrelation curves (N>15). Diffusion coefficients (D1, D2) of S1 and S2 were measured after 2 species fitting of the autocorrelation curves (N>10). Diffusion time (D2) of the mixtures was confined to the diffusion value obtained in the control experiment with Ps89 probe alone. Bars represent mean + SEM. (**c**) Cleavage of caspase-8 (CASP8) and BAP31 was determined by immunoblotting in Jurkat cells treated with PS89 and etoposide (ETO) for 24 or 48 h. (**d**) Co-immunoprecipitation of BAP31 and CASP8 from Jurkat cell lysates after 24 h stimulation with PS89 and ETO. Blots were probed for BAP31 and pro- and intermediate p43/41 CASP8. (**e**) Apoptosis of PS89 and ETO combination treated Jurkat cells in presence of the specific CASP8 inhibitor Z-IETD-FMK after 48 h. (**f**) Apoptosis of BAP31 silenced Hela cells treated for 48 h with PS89 and ETO (6 h post-transfection). Percentage of apoptotic cells was determined by FACS analysis and normalized to controls. Effect of PS89 combination vs. ETO single treatment was analyzed in siCtrl and siBAP31 cells (One way ANOVA, Tukey, $p<0.05$).

Figure 4. Pro-apoptotic crosstalk at the ER-mitochondria interface. (**a**) Intracellular calcium levels of Jurkat cells treated with PS89 and etoposide (ETO) for 24 and 48 h. Fluorescence of Cal-520 stained cells was determined by FACS analysis and mean values normalized towards DMSO control. Dotted grey line represents unstained controls. (**b**) Mitochondrial depolarization of Jurkat cells treated with PS89 and ETO for 24 and 48 h. Percentage of JC-1 stained cells with dissipated vs. intact membrane potential $\Delta\Psi m$ was determined by FACS analysis (populations as shown by FACS dot plots). (**c**) Cytochrome c release from mitochondria to the cytosol. Fractionation of Jurkat cell lysates after 48 h treatment with PS89 and ETO was confirmed by VDAC immunoblot. Stainfree gels served as loading control. (**d**) Intracellular ROS levels of Jurkat cells treated with PS89 and ETO for 24 and 48 h. Fluorescence of Carboxy-H_2DCFDA stained cells was determined by FACS analysis and mean values normalized towards DMSO control. Dotted grey line represents unstained controls. (**e**) Apoptosis of Jurkat vector control (Jurkat/*neo*), Bcl-2 overexpressing (Jurkat/*Bcl-2*) and Bcl-xL overexpressing (Jurkat/*Bcl-xL*) cells treated with ETO and PS89 for 48 h. (**f**) Apoptosis of Jurkat cells treated with ABT-199 (0.5 - 50 µM) in presence or absence of 25 µM PS89. Percentage of apoptotic cells was determined by FACS analysis after 48 h and synergism was calculated using Bliss independence model.

Figure 5. Communication at the ER-mitochondria interface in PS89 combination treatments. For details see text.

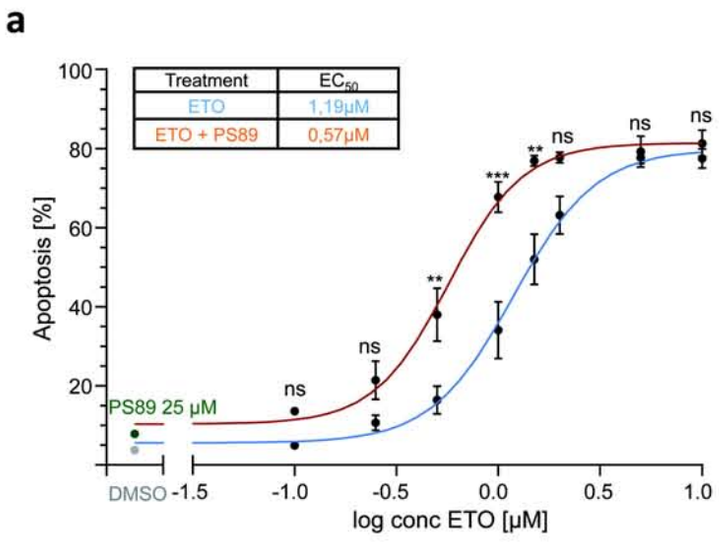

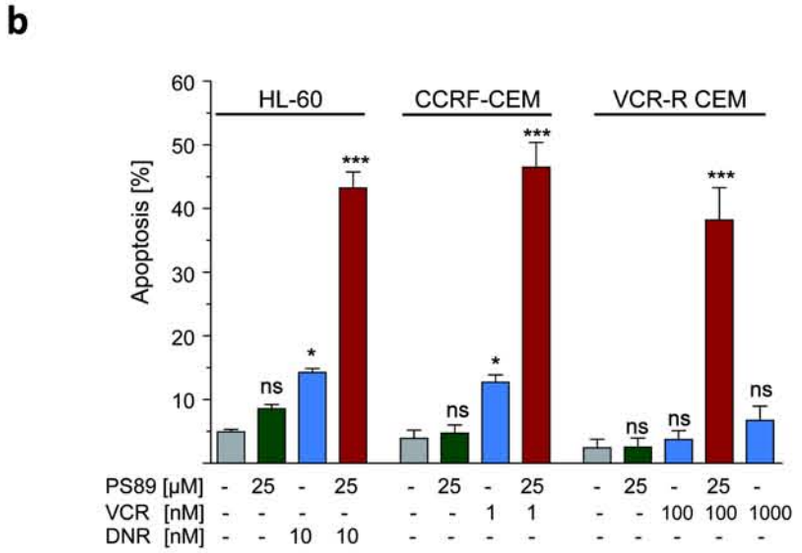

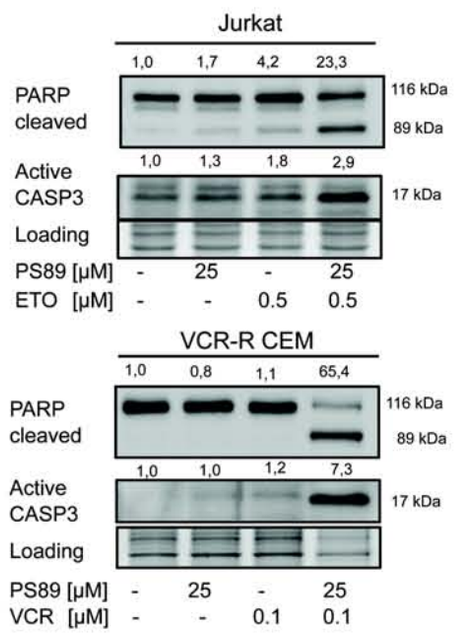

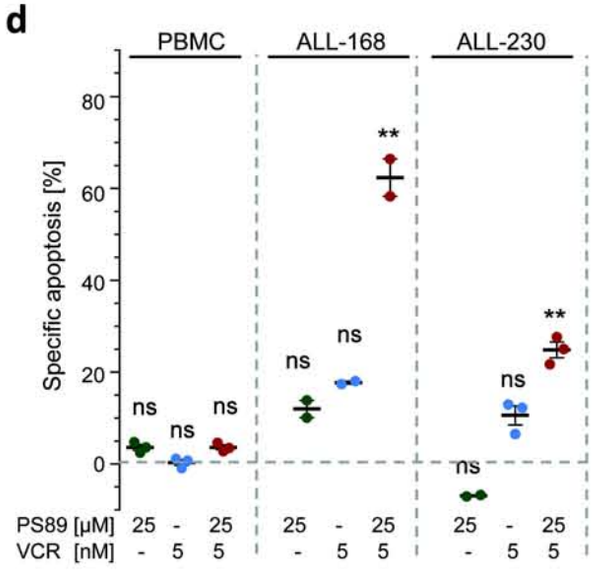

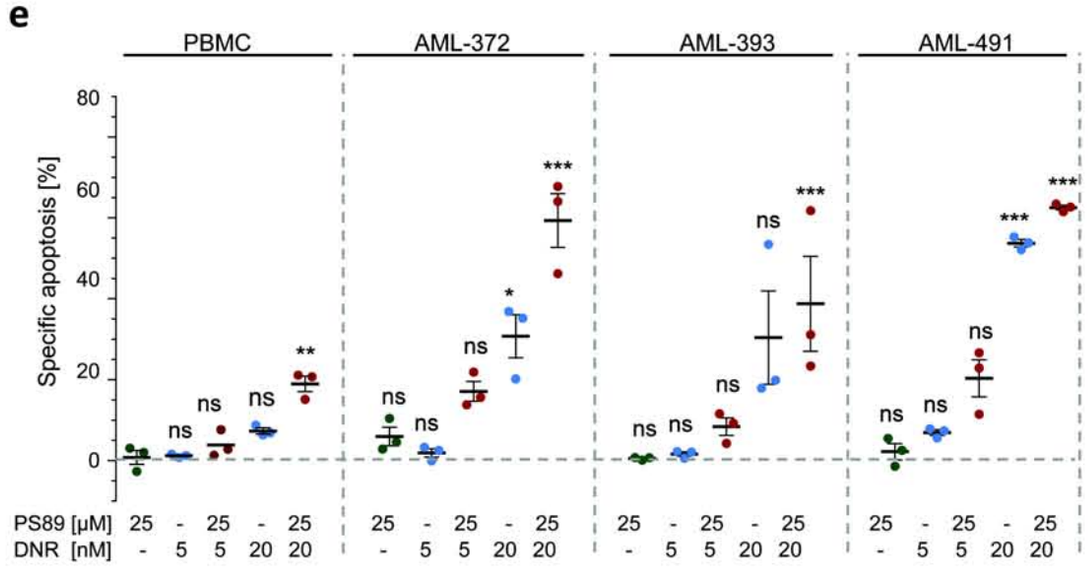

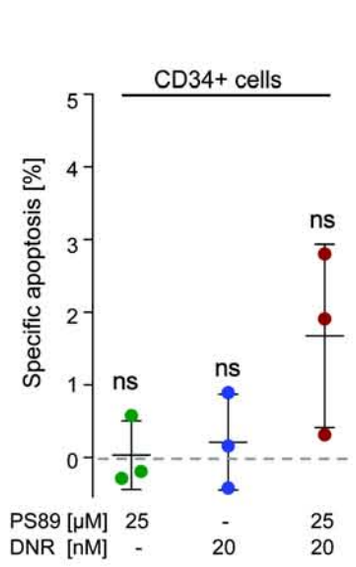

Bliss values (> 1 indicates synergism)	treatment 5nM VCR +PS89	synergistic effect
PBMC	0.9	no
ALL-168	2.3	yes
ALL-230	5.6	yes

Bliss values (> 1 indicates synergism)	treatment 5nM DNR +PS89	treatment 20nM DNR +PS89	synergistic effect
PBMC	2.0	2.4	yes
AML-372	2.2	1.7	yes
AML-393	3.9	1.3	yes
AML-491	2.3	1.1	yes

Fig 1

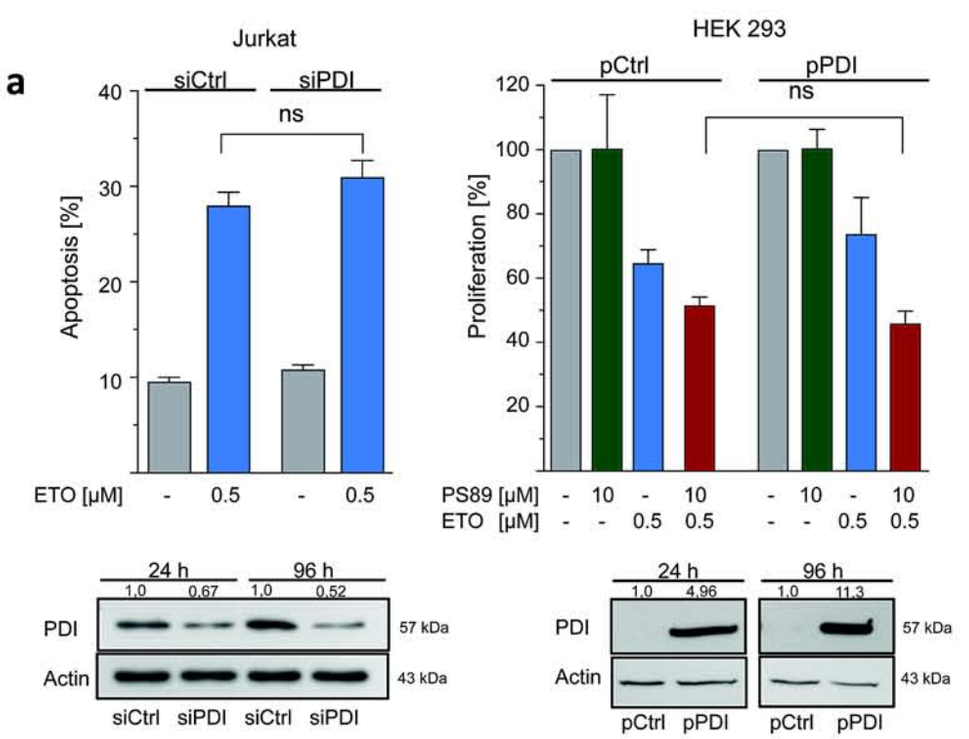

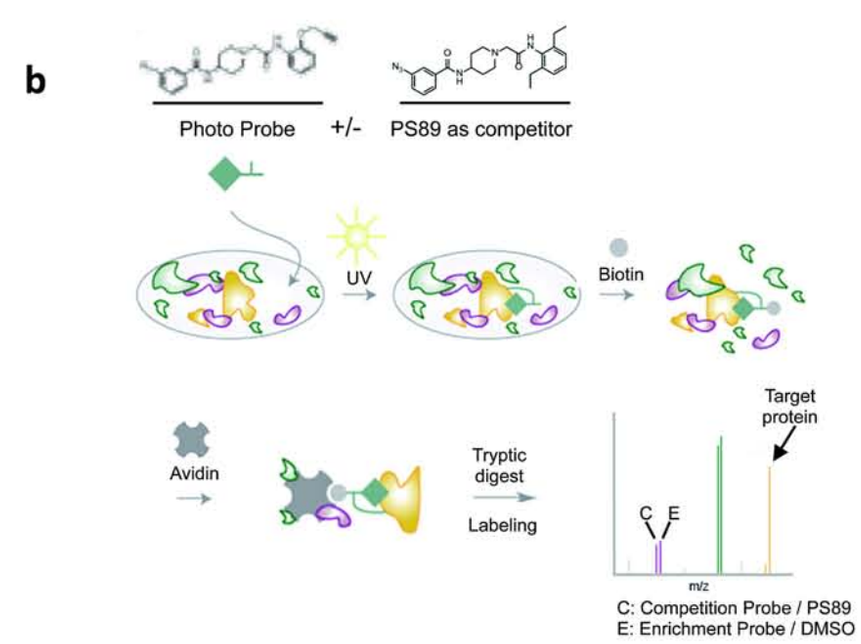

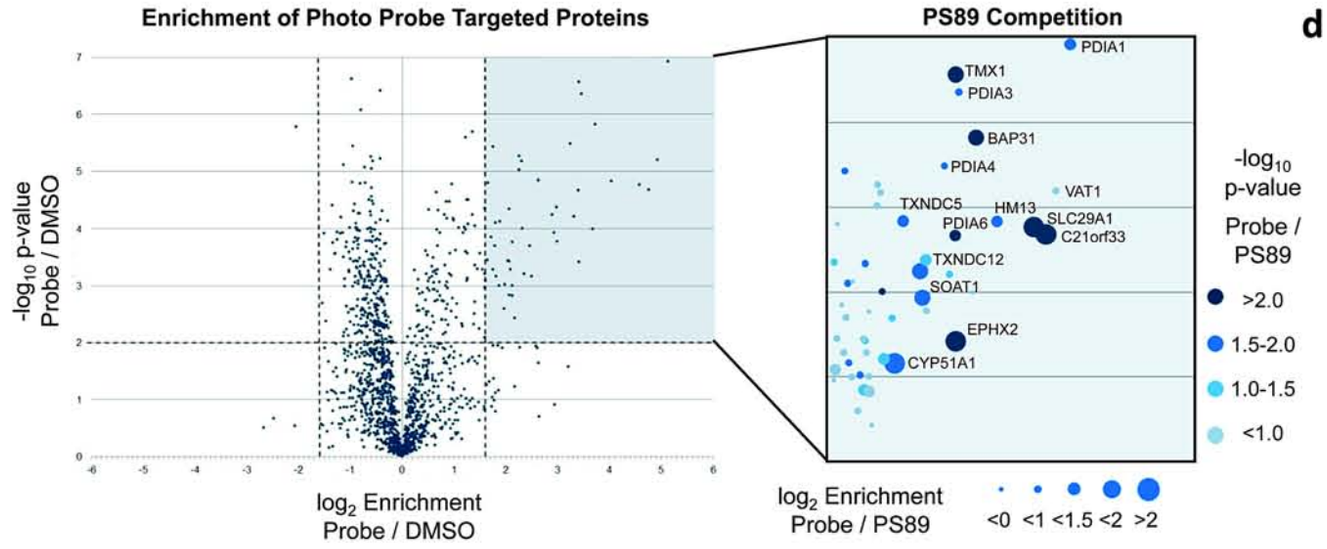

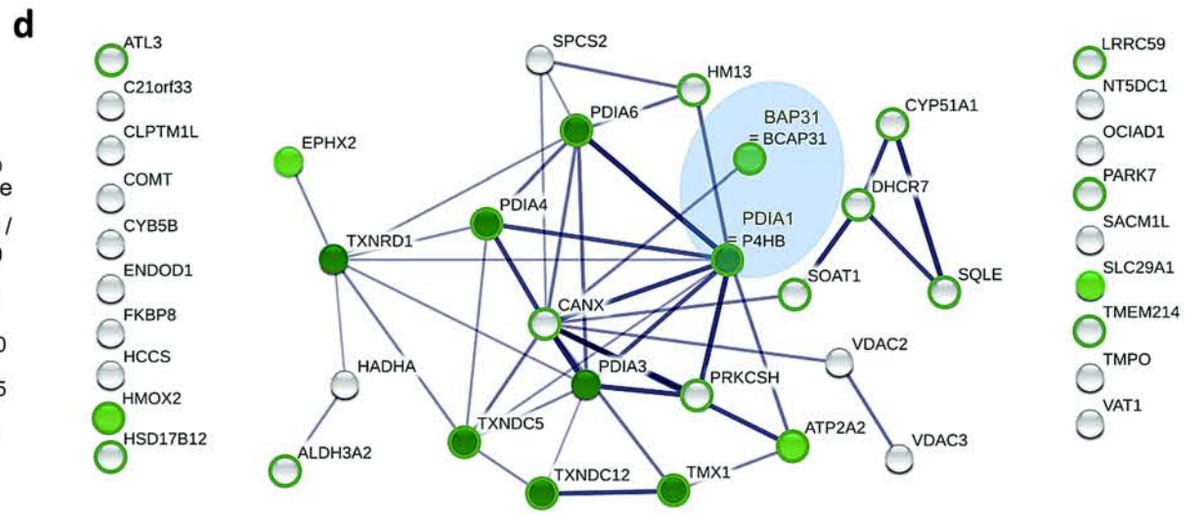

e

Pathway ID	Pathway Description	Count in Gene Set	FDR
Cellular Component (GO)			
GO:0005783	Endoplasmic Reticulum	22	5.9e-12
Biological Process (GO)			
GO:0045454	Cell Redox Homeostasis	8	6.7e-09
GO:0019725	Cellular Homeostasis	13	9.1e-07

Fig 2

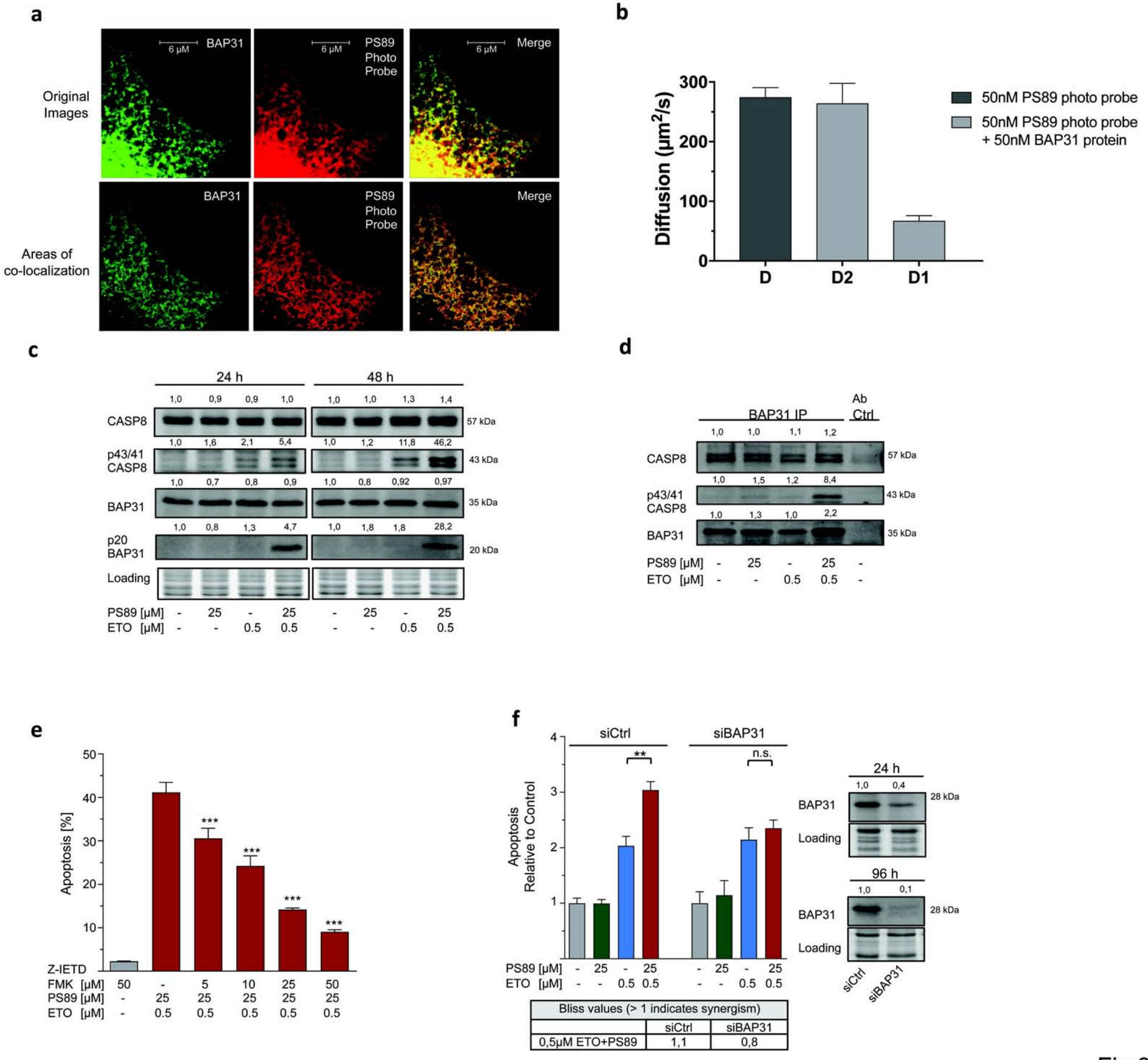
a
Original Images
Areas of co-localization
BAP31
PS89 Photo Probe
Merge
6 µM
b
Diffusion (µm²/s)
300
200
100
0
D
D2
D1
50nM PS89 photo probe
50nM PS89 photo probe + 50nM BAP31 protein
c
24 h
48 h
CASP8
p43/41 CASP8
BAP31
p20 BAP31
Loading
57 kDa
43 kDa
35 kDa
20 kDa
PS89 [µM]
ETO [µM]
d
BAP31 IP
Ab Ctrl
CASP8
p43/41 CASP8
BAP31
PS89 [µM]
ETO [µM]
e
Apoptosis [%]
Z-IETD
FMK [µM]
PS89 [µM]
ETO [µM]
f
siCtrl
siBAP31
Apoptosis Relative to Control
**
n.s.
24 h
96 h
BAP31
Loading
28 kDa
siCtrl
siBAP31
Bliss values (> 1 indicates synergism)
0,5µM ETO+PS89
1,1
0,8

Fig 3

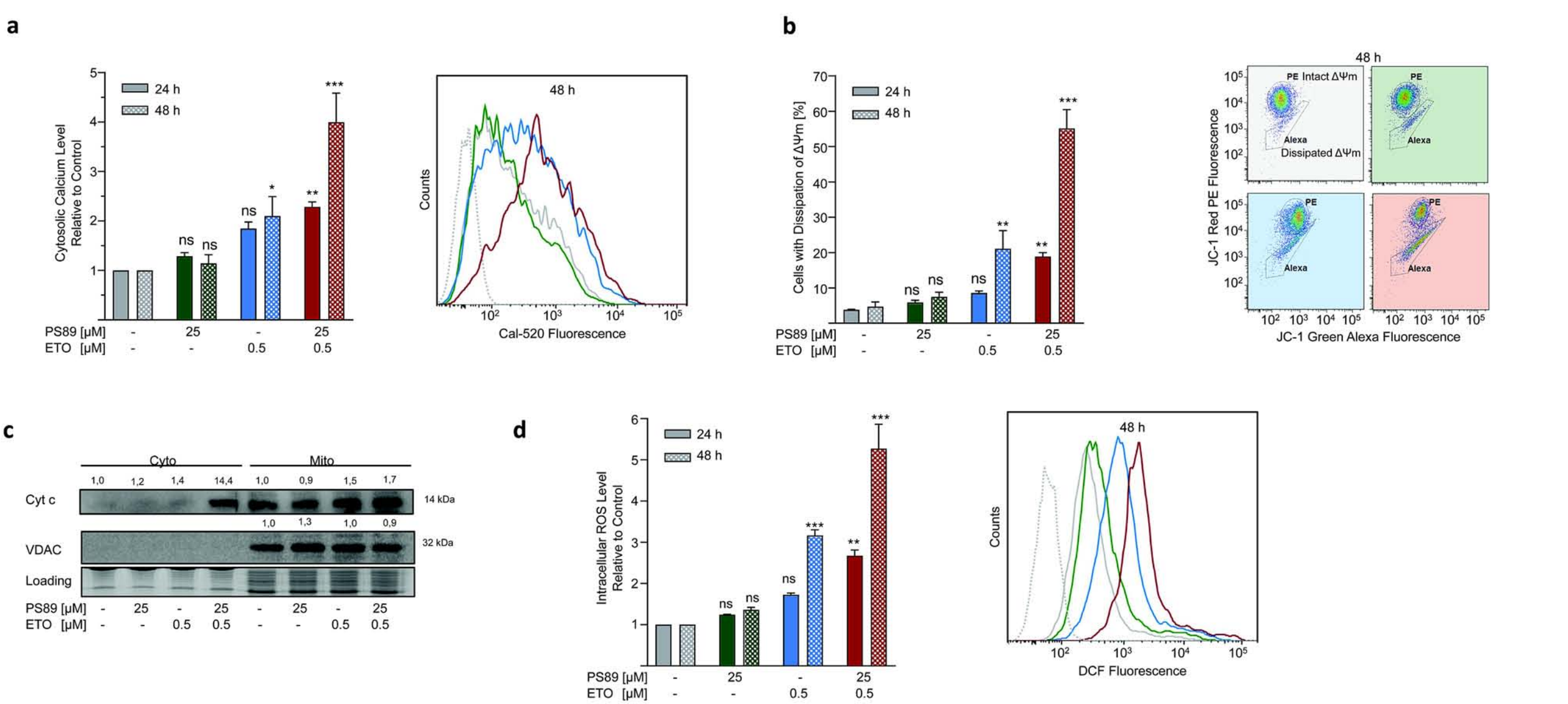
a
24 h
48 h
Cytosolic Calcium Level Relative to Control
ns
ns
ns
*
**
***
PS89 [µM] - 25 - 25
ETO [µM] - - 0.5 0.5
48 h
Counts
Cal-520 Fluorescence
b
24 h
48 h
Cells with Dissipation of ΔΨm [%]
PS89 [µM] - 25 - 25
ETO [µM] - - 0.5 0.5
48 h
PE Intact ΔΨm
Alexa
Dissipated ΔΨm
JC-1 Red PE Fluorescence
JC-1 Green Alexa Fluorescence
c
Cyto
Mito
Cyt c
14 kDa
VDAC
32 kDa
Loading
PS89 [µM] - 25 - 25 - 25 - 25
ETO [µM] - - 0.5 0.5 - - 0.5 0.5
d
24 h
48 h
Intracellular ROS Level Relative to Control
PS89 [µM] - 25 - 25
ETO [µM] - - 0.5 0.5
48 h
Counts
DCF Fluorescence
e
PS89 25 µM + ETO 0.5 µM
Apoptosis [%]
Jurkat/neo
Jurkat/Bcl-2
Jurkat/Bcl-xL
Jurkat
neo Bcl-2
Bcl-2
28 kDa
Loading
Jurkat
neo Bcl-xL
Bcl-xL
30 kDa
Loading
f
Treatment | EC50
ABT-199 | 9,8µM
ABT-199 + PS89 | 3,7µM
PS89 25 µM
DMSO
Apoptosis [%]
log conc ABT-199 [µM]

Fig 4

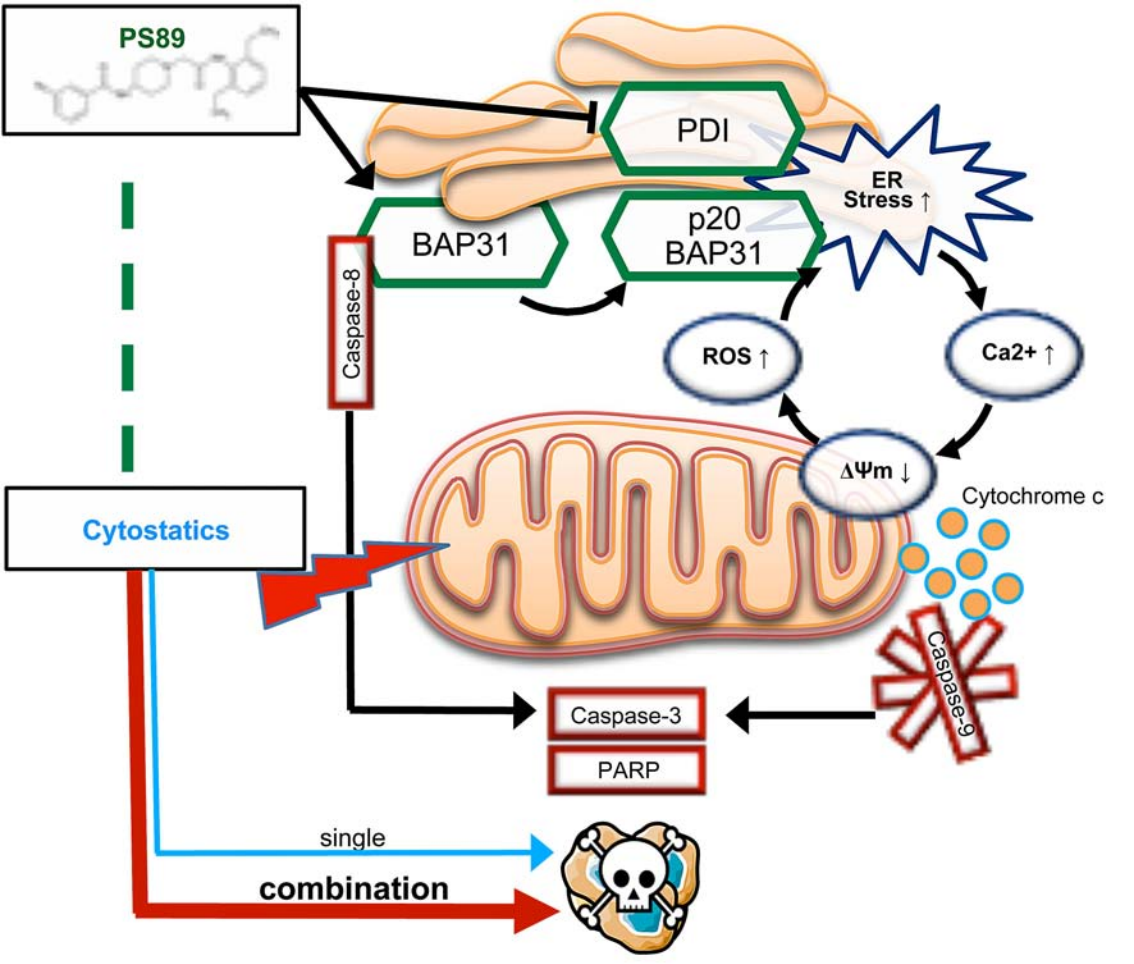
PS89
PDI
ER Stress ↑
BAP31
p20 BAP31
Caspase-8
ROS ↑
Ca2+ ↑
ΔΨm ↓
Cytochrome c
Cytostatics
Caspase-9
Caspase-3
PARP
single
combination

Fig 5

Targeting the ER-Mitochondria Interface Sensitizes Leukemia Cells Towards Cytostatics

Fabian Koczian, Olga Nagło, Jan Vomacka, Binje Vick, Phil Servatius, Themistoklis Zisis, Britta Hettich, Uli Kazmaier, Stephan A. Sieber, Irmela Jeremias, Stefan Zahler, Simone Braig

SUPPLEMENTARY METHODS

Compounds
PS89 was synthesized as described previously.(1) The PS89 photo probe was labeled with a rhodamine reporter dye by click chemistry (5-TAMRA-Azide; Jena Bioscience, Jena, Germany). Etoposide, daunorubicin, 6-mercaptopurine, dexamethasone and vincristine were purchased from Sigma Aldrich (St Louis, MO, USA). ABT-199 was obtained from LKT Laboratories (St Paul, MN, USA), Z-IETD-FMK from R&D Systems (Minneapolis, MN, USA) and QVD-OPh from Merck Millipore (Darmstadt, Germany).

Apoptosis assay
Apoptosis was determined according to Nicoletti *et al*.(2) In brief, stimulated cells were stained with 50 µg/ml propidium iodide (PI, Sigma Aldrich) in 0.1% Triton X-100 permeabilization buffer and percentage of apoptotic cells at subG1 was determined using a FACSCanto II flow cytometer (BD, Franklin Lakes, NJ, USA) and FlowJo software v7.6.5 (Tree Star, Ashland, OR, USA). Apoptosis of daunorubicin treated HL-60 cells was determined using YO-PRO-1 nucleic acid stain.
PDX cells and PBMCs were analyzed with identical equipment and the percentage of viable or apoptotic cells, respectively, was determined by forward/side scatter (FSC/SSC) gating as previously described (3). For cell death analysis of CD34+ cells, PBMCs were isolated and stained with FITC conjugated-anti-CD34 antibody. Propidium iodide was used to determine the cell death of at least 25000 CD34 positive cells by flow cytometry. Specific apoptosis was calculated as follows: [(experimental apoptosis (%) - spontaneous apoptosis (%)) / (100% - spontaneous apoptosis (%))] x 100

Proliferation assay
Cells were allowed to proliferate for 72 h in presence or absence of stimulants and stained with CellTiter-Blue reagent (Promega, Fitchburg, WI, USA) for 4 h. Fluorescence was measured on a SpectraFluor Plus microplate reader (Tecan, Männedorf, Switzerland) and normalized towards DMSO control.

Western Blot
Chemiluminescent western blotting was performed according to standard procedures. Protein amount was quantified by BCA assay (Uptima BC Assay Kit, Interchim, Montlucon, France) and equal protein load was determined by actin staining or stainfree detection (4) using a ChemiDoc Touch Imaging System (Bio-Rad, Hercules, CA, USA), as indicated. Proteins were transferred to Amersham PVDF membranes (GE Healthcare) by tank blotting. Densitometric quantification of the band intensity of 3 independent western blot experiments was performed by using Image J software.

Antibodies for Western blot

Primary antibody	Origin	Supplier
Actin Clone C4	Mouse	Millipore, Darmstadt, Germany
BAP31 B-10	Mouse	Santa Cruz, Dallas, TX, USA
BAP31 C-15	Goat	Santa Cruz, Dallas, TX, USA
Bcl-2 2872	Rabbit	Cell Signaling, Danvers, MA, USA
Bcl-xL 2762	Rabbit	Cell Signaling, Danvers, MA, USA
Caspase-3, Active C8487	Rabbit	Sigma Aldrich, St Louis, MO, USA
Caspase-8 1C12	Mouse	Cell Signaling, Danvers, MA, USA
Cytochrome c 4272	Rabbit	Cell Signaling, Danvers, MA, USA
PARP 9542	Rabbit	Cell Signaling, Danvers, MA, USA
PDI C81H6	Rabbit	Cell Signaling, Danvers, MA, USA
VDAC 4866	Rabbit	Cell Signaling, Danvers, MA, USA

Secondary antibody	Origin	Supplier
Anti-goat IgG, HRP 705-035-147	Donkey	Dianova, Hamburg, Germany
Anti-mouse IgG, HRP 7076	Goat	Cell Signaling, Danvers, MA, USA
Anti-rabbit IgG, HRP 172-1019	Goat	Bio-Rad, Hercules, CA, USA

Transfection
Gene silencing was performed using GenaxxoFect reagents (Genaxxon, Ulm, Germany) according to manufacturer's instructions and ON-TARGET*plus* SMARTpool siRNA (GE Dharmacon, Lafayette, CO, USA) against human PDIA1 and BCAP31. Overexpression of PDIA1 was performed with FuGene HD reagent (Promega, Fitchburg, WI, USA). PDI vector was kindly provided by W. Ou (Bethesda, MD, USA).(5)

Target network analysis
Protein-protein interaction network analysis was performed using STRING v10 (6) with subsequent refinement of functional enrichment by Gene Ontology (GO) classification.(7)

Confocal microscopy
Hela cells were incubated with the PS89 photo probe followed by UV crosslinking to cellular targets at 365 nm and coupling of a rhodamine reporter dye by click chemistry (5-TAMRA-Azide; Jena Bioscience, Jena, Germany). BAP31 was subsequently stained using anti-BAP31 HPA003906 (Sigma Aldrich) and goat anti-rabbit Alexa 488 (Thermo Fisher, Waltham, MA, USA) according to Prestige Antibody IF procedure. Confocal microscopy was performed on a Leica SP8 LSM system (Leica, Wetzlar, Germany) and co-localization was evaluated using Leica LAS X software.

Fluorescence Correlation Spectroscopy (FCS)
FCS measurements were performed on a Leica TCS SP8 SMD microscope combined with a Picoquant LSM Upgrade Kit. For all measurements, 63x Zeiss water immersion lens and ibidi 8 well µ-slides with glass bottoms were used. The effective volume (V_{eff}) and structure parameter (κ) were measured at the start of each experiment using 1nM ATTO488 dye solution (ATTO-TEC GmbH, Siegen, Germany). Ten or more different points were measured in every well for 45 s per point. The samples included two different concentrations (50 nM and 250 nM) of the freely diffusing PS89 probe in buffer and two different concentration ratios [S1: 50nM/50nM, (1:1), S2: 50 nM/200 nM, (1:4)] of the PS89 plus the recombinant human BAP31 protein (Abcam plc, Cambridge, UK), respectively. All solutions were diluted using 50 mM Tris-HCL, pH = 8 buffer with a 5% DMSO. All concentrations were also verified with nanodrop spectrophotometer. FCS curves were analyzed using the Picoquant SymPhoTime V 5.2.4.0 software. Control measurements to determine the diffusion time and concentration of PS89 were fitted with a single diffusing species and a triplet state (eq. 1). Subsequent measurements to determine the diffusion time and concentration of PS89+BAP31, were fitted for two diffusing species and a triplet state (eq. 1). In this case, one of the two species diffusion times was confined to the diffusion time of PS89 obtained in the control experiments.

$$G_{3D}(\tau) = \frac{1}{N} \cdot \left(1 + \frac{T}{1-T} e \frac{\tau}{\tau_t}\right) . \left(1 + \frac{4D \cdot \tau}{{\omega_r}^2}\right)^{-1} \cdot \left(1 + \frac{4D \cdot \tau}{{\omega_z}^2}\right)^{-\frac{1}{2}}$$

$$V_{Eff,3D} = \pi^{\frac{3}{2}} . {w_0}^2 . z_0 \quad ; \quad D_{3D} = \frac{{w_0}^2}{4\tau} \quad ; \quad < C > = \frac{<N>}{V_{Eff} \cdot N_A} \quad (1)$$

Co-immunoprecipitation
Preparation of cell lysates (Triton-X lysis buffer, 500 µg protein per sample determined by BCA assay) and co-IP using the µMACS Protein G MicroBeads kit (Miltenyi Biotech, Bergisch Gladbach, Germany) was performed according to manufacturer's instructions. Precipitation: Goat anti-BAP31 C-15 (Santa Cruz). Detection: Mouse anti-BAP31 B-10 (Santa Cruz) and Mouse anti-CASP8 1C12 (Cell Signaling).

Flow cytometric analysis of calcium, MMP and ROS
The following dyes were used for fluorescence staining. Calcium: Cal-520 (AAT Bioquest, Sunnyvale, CA, USA); Mitochondrial membrane potential (MMP): JC-1 (Enzo, Farmingdale, NY; USA); Reactive oxygen species (ROS): Carboxy-H_2DCFDA (Thermo Fisher). PI counterstaining was used to exclude

dead cells. Sample preparation was performed according to manufacturers' instructions and cells were analyzed on a FACSCanto II flow cytometer (BD).

Cell cycle analysis
Cellular DNA content was examined by propidium iodide staining and flow cytometry.(2) Cell cycle analysis was performed using FlowJo software v7.6.5 (Tree Star, Ashland, OR, USA).

Colony formation assay
Jurkat and VCR-R CEM were stimulated for 4 h, washed with PBS and reseeded at a density of 5.000 cells/ml in 0.4% methylcellulose and 40% FCS supplemented medium to grow into colonies. After 7 or 5 days of proliferation, respectively, colonies were stained with MTT (0.25 mg/ml) for 3 h. Images of each well were analyzed with ImageJ software (open source) and the number of colony forming units (CFU) per well was normalized towards DMSO control. HL-60 cells were treated for 24h with PS89 and 6-MP, washed and reseeded (2000 cells/ml) in methylcellulose medium (Human Methylcellulose complete media, R&D Systems, Minneapolis, MN, USA). Clonogenic growth was monitored by counting the colonies after 7 days, respectively.

Data collection and statistics
Data from at least three independent experiments are expressed as mean ± SEM and statistical analysis was performed with GraphPad Prism 7 (GraphPad Software, San Diego, CA, USA). For Western blot and confocal microscopy, representative images of at least three independent data sets are shown. Synergism was calculated according to the Bliss independence model (8) as described in the following equitation: $Y_P = Y_{ab}/(Y_a + Y_b - Y_aY_b)$, where Ya is the cytotoxic effect of drug a and Yb the effect of drug b. $Y_P > 1$: synergy, $Y_P < 1$: antagonism, $Y_P = 1$: additivity.

SUPPLEMENTARY REFERENCES

1. Eirich J, Braig S, Schyschka L, et al. A small molecule inhibits protein disulfide isomerase and triggers the chemosensitization of cancer cells. Angewandte Chemie International Edition. 2014;53(47): 12960-12965.
2. Nicoletti I, Migliorati G, Pagliacci M, et al. A rapid and simple method for measuring thymocyte apoptosis by propidium iodide staining and flow cytometry. Journal of immunological methods. 1991;139(2): 271-279.
3. Ehrhardt H, Schrembs D, Moritz C, et al. Optimized anti–tumor effects of anthracyclines plus Vinca alkaloids using a novel, mechanism-based application schedule. Blood. 2011;118(23): 6123-6131.
4. Ladner CL, Yang J, Turner RJ, et al. Visible fluorescent detection of proteins in polyacrylamide gels without staining. Analytical biochemistry. 2004;326(1): 13-20.
5. Ou W, Silver J. Role of protein disulfide isomerase and other thiol-reactive proteins in HIV-1 envelope protein-mediated fusion. Virology. 2006;350(2): 406-417.
6. Szklarczyk D, Franceschini A, Wyder S, et al. STRING v10: protein–protein interaction networks, integrated over the tree of life. Nucleic acids research. 2014: gku1003.
7. Consortium GO. Gene ontology consortium: going forward. Nucleic acids research. 2015;43(D1): D1049-D1056.
8. Bliss CI. The calculation of microbial assays. Bacteriol Rev. 1956 Dec;20(4): 243-258.

SUPPLEMENTARY FIGURE LEGENDS

Supplementary Figure S1. (**a**) Jurkat cells were treated with PS89 and etoposide (ETO) for 48 h, permeabilized and stained with propidium iodide. Cell cycle was analyzed by flow cytometry. (**b**) Jurkat cells were incubated with ETO and allowed to proliferate for 72 h in presence or absence of PS89. Viable cells were determined by CellTiter-Blue staining and normalized towards DMSO control. (**c**) Jurkat cells stimulated for 4 h with PS89 and ETO were washed and reseeded at low density (5.000 cells/ml) in medium with increased viscosity. The number of colonies was quantified after 7 days of proliferation and normalized towards DMSO control. (**d**) Jurkat or (**e**) HL-60 cells were treated with increasing concentrations of 6-mercaptopurine in combination with 25µM PS89. After 48h apoptosis rate was determined by FACS measurements. (**f)** Combined treatment of HL-60 and Jurkat cells with indicated concentrations of dexamethasone (DEX) and PS89 for 48h and analysis of apoptosis rate. (**g**) Vincristine resistant CEM cells stimulated for 4 h with PS89 and vincristine (VCR) were washed and reseeded in medium with increased viscosity. After 5 days, the number of colonies was quantified and normalized towards DMSO control. (**h**) HL-60 cells were treated for 24h with PS89 and 6-mercaptopurine and reseeded in low density in methylcellululose medium. Clonogenic growth was monitored by counting the colonies after 7 days.

Supplementary Figure S2. CCRF-CEM and HL-60 cells were cultured for 24h in drug supplemented medium as indicated and cleavage of PARP and caspase 3 activation was analyzed by Western Blotting.

Supplementary Figure S3. Vincristine resistant (VCR-R) CEM cells were treated with PS89 and VCR in presence or absence of the pan-caspase inhibitor Q-VD. Percentage of apoptotic cells was determined by FACS analysis after 48 h.

Supplementary Figure S4. PDI silenced Jurkat cells (siRNA transfection, 24 h) were incubated with etoposide (ETO) and allowed to proliferate for 72 h. Viable cells were determined by CellTiter-Blue staining and normalized towards DMSO control. PDI expression was analyzed by immunoblotting as shown in Figure 2a.

Supplementary Figure S5. Control of secondary antibody background staining, immuno-fluorescence of BAP31 primary and goat anti-rabbit Alexa 488 secondary antibodies and rhodamine reporter dye background staining (5-TAMRA-Azide) with and without PS89 photo probe after UV crosslinking and coupling to the rhodamine reporter using equal settings as in Fig 3a. Nuclei were stained with Hoechst 33342.

Supplementary Figure S6. (a) Example of FCS autocorrelation curves and residual plots for all measured samples. (**b**) Two different concentrations (50 nM, 250 nM) of the freely diffusing PS89 in buffer solution were analyzed by single-point FCS. Diffusion coefficients were measured after 1 species fitting of the autocorrelation curves (N>15). Bars represent mean + SEM. (**c**) Diffusion values of the two different species of PS89 in combination with 200nM BAP31. (**d**) Concentration values for all measured samples acquired by single-point FCS were measured and verified after 1 or 2 species fitting of the autocorrelation curves (N>15, N>10). Bars represent mean + SEM.

Supplementary Figure S7. (**a**) CEM cells or (**b**) ALL patient derived xenograft (PDX) cells were treated with PS89 and vincristine for indicated time points and expression and cleavage of caspase 8 and BAP31 was analyzed by western blotting.

Supplementary Figure S8. Normalization of protein amounts of cleaved caspase 8 to immunoprecipitated BAP31 in Jurkat cells treated with PS89 and etoposide.

Supplementary Figure S9. Caspase-8 deficient (CASP8 -/-) or wildtype Jurkat cells were treated with PS89 25 µM and etoposide (ETO 250 nM or 500 nM, respectively). Percentage of apoptotic cells was determined by FACS analysis after 48 h. Knockout of CASP8 was verified by immunoblotting.

Supplementary Figure S10. Cytosolic calcium levels in PS89, vincristine or daunorubicin treated (**a**) CCRF- CEM, (**b**) HL-60 and (**c**) ALL PDX cells were analyzed by FACS measurements after 24h or 48h, as indicated.

Supplementary Figure S11. Cytochrome release into the cytosol after treatment of CCRF-CEM cells with PS89 and vincristine was determined after 48h by cytosol-mitochondrial fractionation and western blotting.

Supplementary Figure S12. (**a)** CCRF-CEM and (**b**) HL-60 cells were treated with PS89 and cytostatics. Intracellular ROS levels were evaluated by FACS measurements after 24h and 48h.

SUPPLEMENTARY TABLES

Supplementary Table S1. (a,b) Synergistic interaction of PS89 and cytostatics in cells treated according to Figure 1a and 1b was evaluated by using the Bliss independence model.

Supplementary Table S2. Classification and cytogenetic characteristics of PDX samples.

Supplementary Table S3. (a,b) Respective p-values of PBMCs, CD34+, ALL and AML patient samples treated with PS89 and vincristine or daunorubicin were calculated by ordinary one-way ANOVA test. Green fields indicate statistically significant effects (p-values <0,05). **(c)** The Brown-Forsythe statistical test demonstrates that group variances of CD34postive treated cells as shown in Fig 1f are statistically equal.

Supplementary Table S4. List of PS89 target proteins identified by ABPP (n=42) matching defined criteria: (1) Probe / DMSO: >3-fold enrichment (log_2 Probe / DMSO >1.6) and -log_{10} p-value >2. (2) Probe / PS89 log_2 enrichment >0. Ranks were assigned according to the degree of enrichment and their reproducibility. The overall score was calculated as the average of all ranks with double weighting the Probe/PS89 competition values.

Supplementary Table S5. Synergistic interaction of PS89 and ABT-199 in Jurkat cells was evaluated by using the Bliss independence model.

Supplement

S1

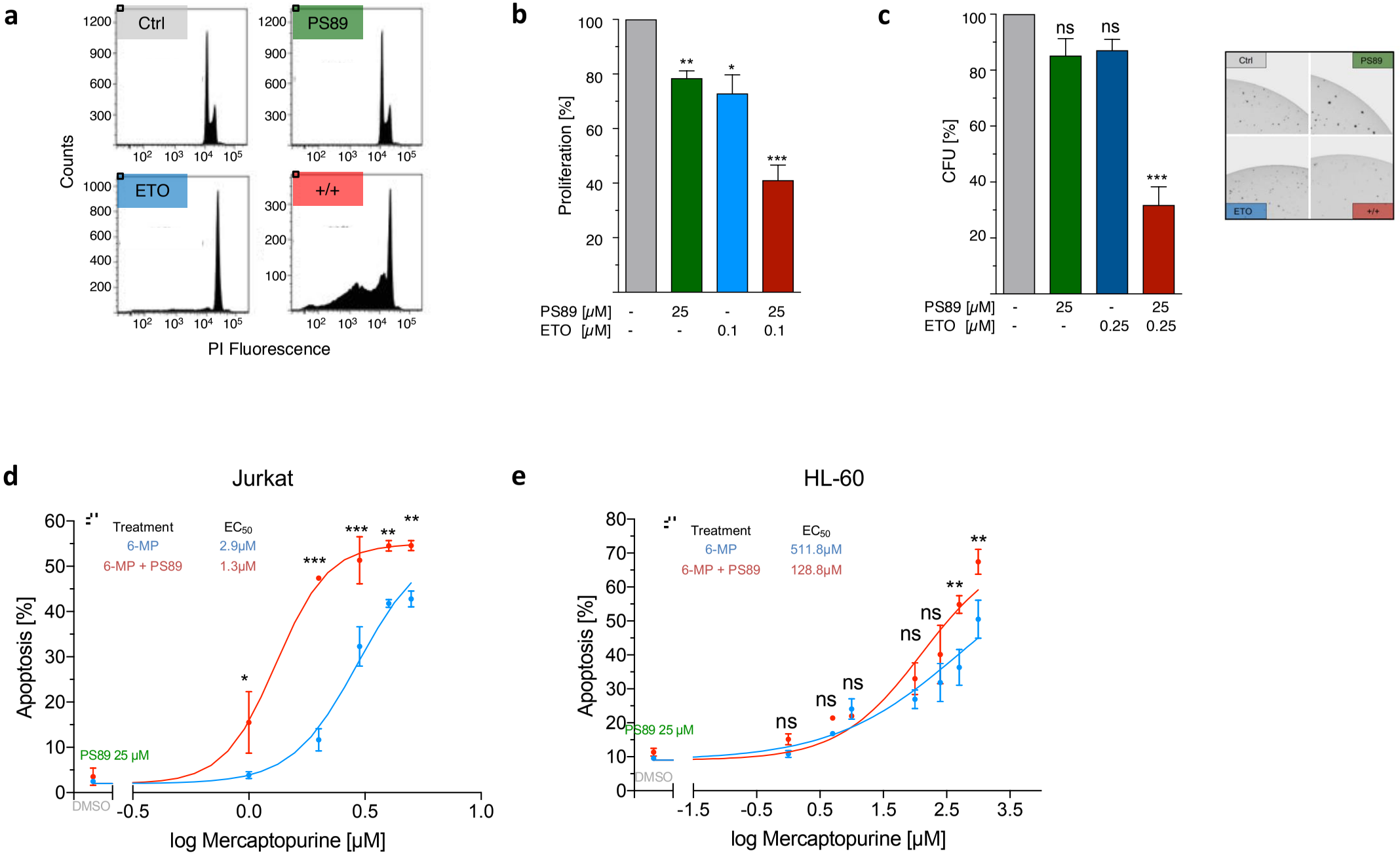

S1

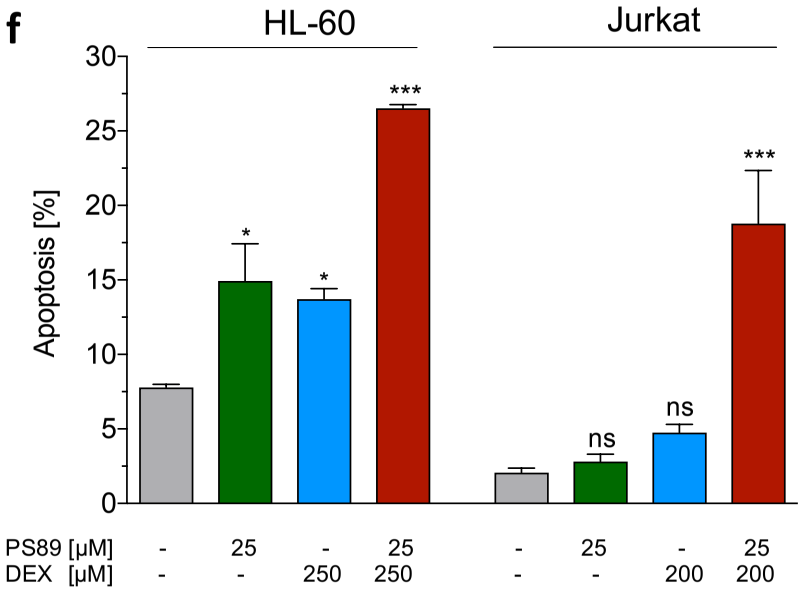
f
HL-60
Jurkat
Apoptosis [%]
0
5
10
15
20
25
30
*
*
***
ns
ns
***
PS89 [µM] - 25 - 25 - 25 - 25
DEX [µM] - - 250 250 - - 200 200

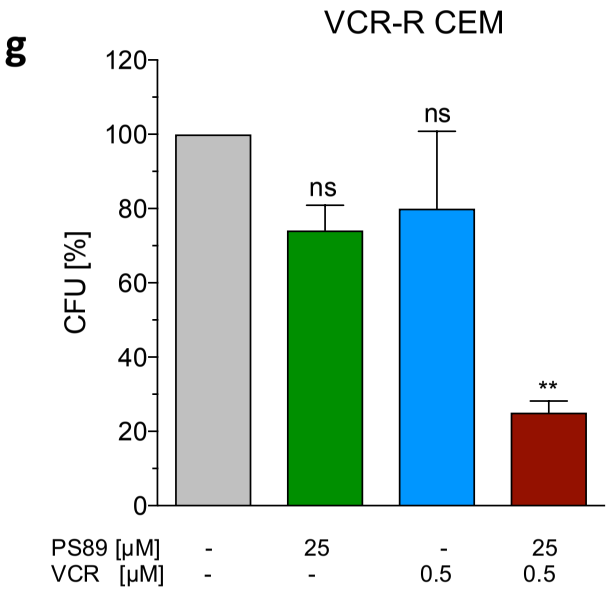
g
VCR-R CEM
CFU [%]
0
20
40
60
80
100
120
ns
ns
**
PS89 [µM] - 25 - 25
VCR [µM] - - 0.5 0.5

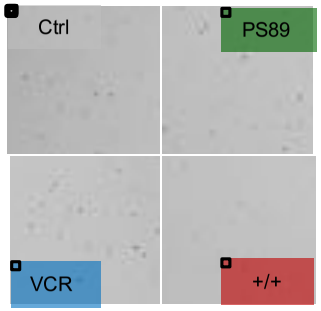
Ctrl
PS89
VCR
+/+

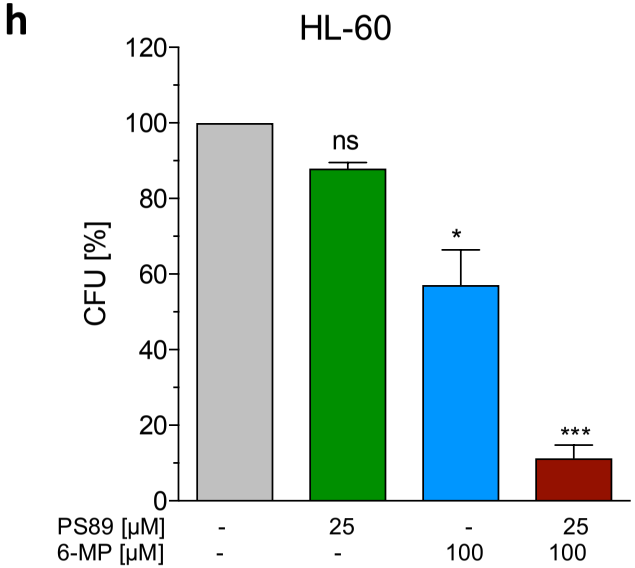
h
HL-60
CFU [%]
0
20
40
60
80
100
120
ns
*
***
PS89 [µM] - 25 - 25
6-MP [µM] - - 100 100

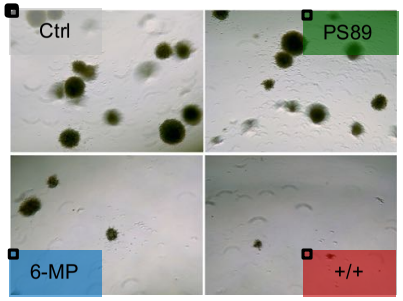
Ctrl
PS89
6-MP
+/+

S2

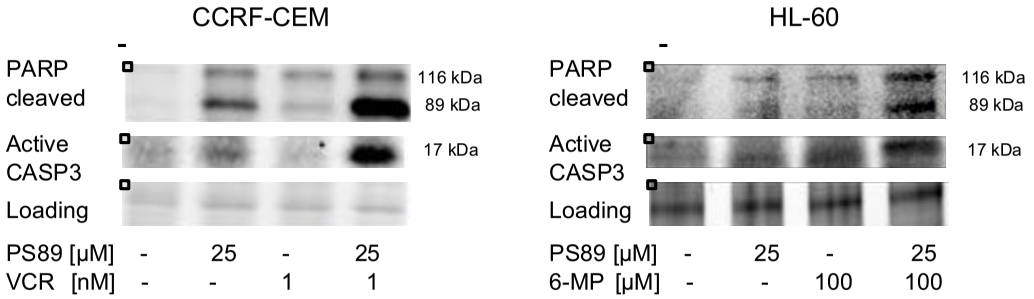
CCRF-CEM
PARP cleaved
116 kDa
89 kDa
Active CASP3
17 kDa
Loading
PS89 [µM] - 25 - 25
VCR [nM] - - 1 1
HL-60
PARP cleaved
116 kDa
89 kDa
Active CASP3
17 kDa
Loading
PS89 [µM] - 25 - 25
6-MP [µM] - - 100 100

S3

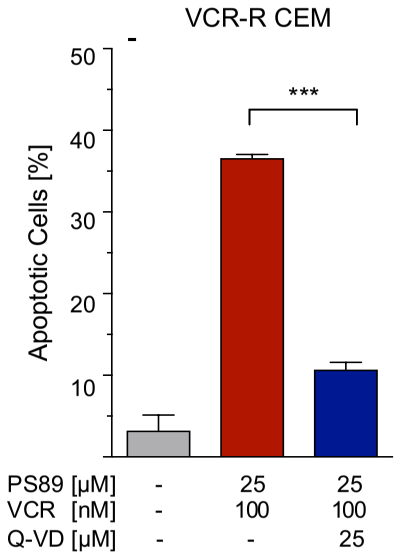
VCR-R CEM
Apoptotic Cells [%]
50
40
30
20
10
***
PS89 [µM] - 25 25
VCR [nM] - 100 100
Q-VD [µM] - - 25

S4

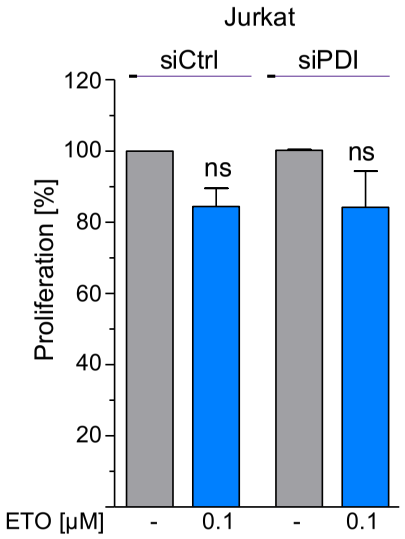
Jurkat
siCtrl
siPDI
Proliferation [%]
120
100
80
60
40
20
ns
ns
ETO [µM] - 0.1 - 0.1

S5

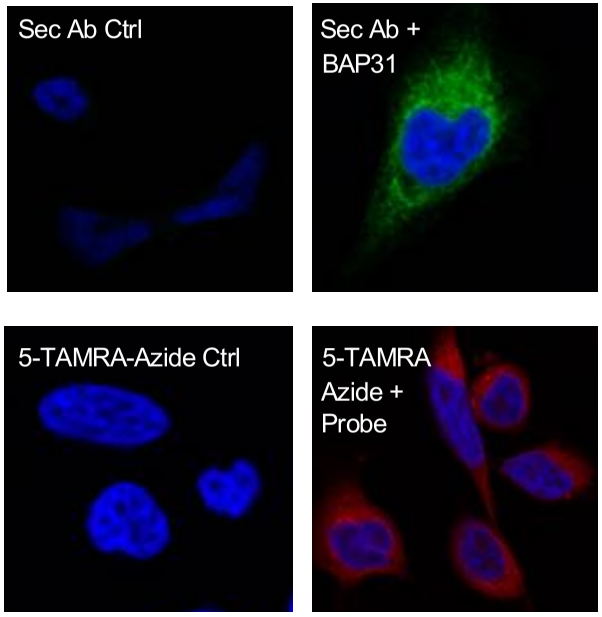
Sec Ab Ctrl
Sec Ab + BAP31
5-TAMRA-Azide Ctrl
5-TAMRA Azide + Probe

S6

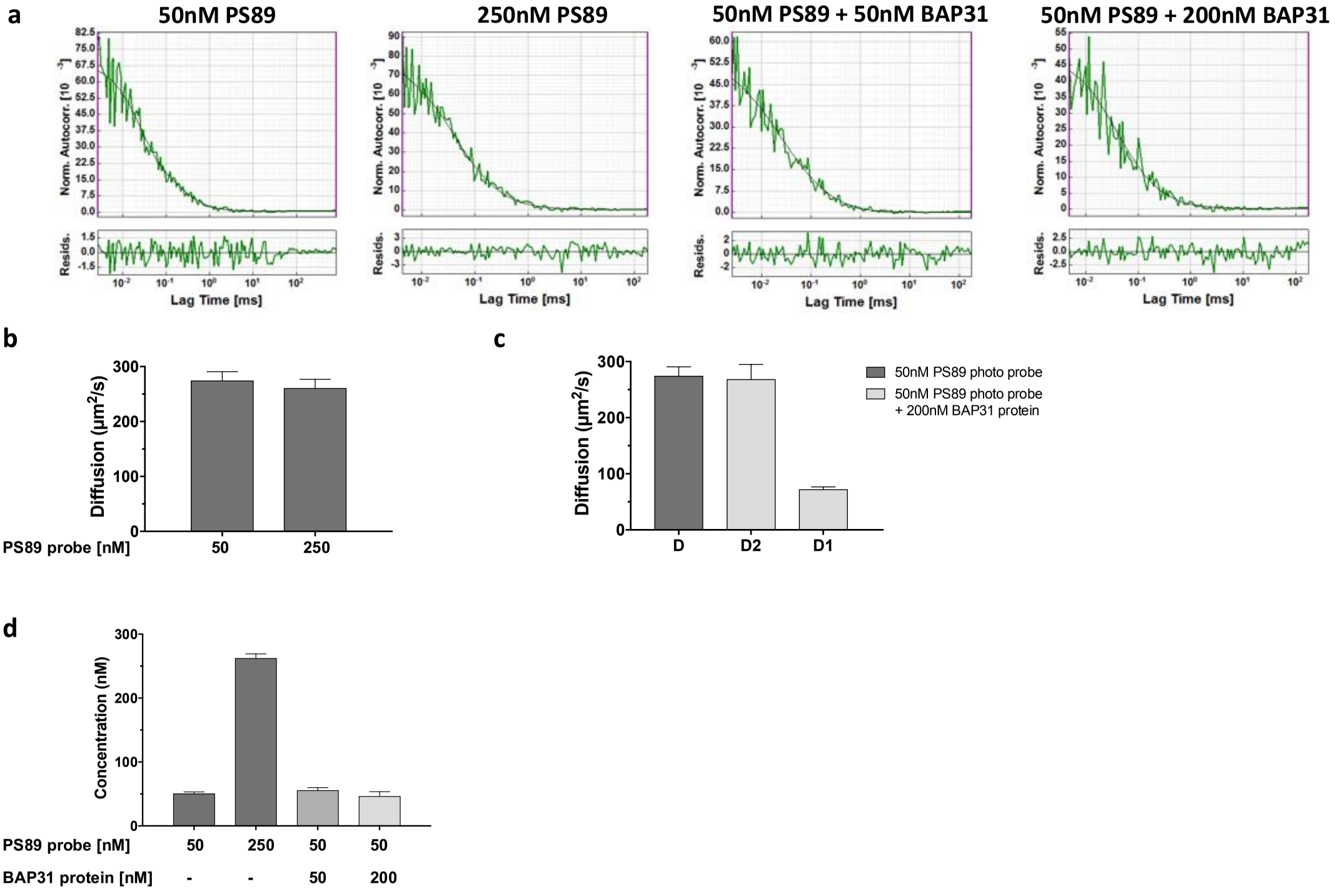
a
50nM PS89
250nM PS89
50nM PS89 + 50nM BAP31
50nM PS89 + 200nM BAP31
Norm. Autocorr. [10 -3]
Resids.
Lag Time [ms]
b
Diffusion (μm²/s)
PS89 probe [nM]
50
250
c
Diffusion (μm²/s)
50nM PS89 photo probe
50nM PS89 photo probe
+ 200nM BAP31 protein
D
D2
D1
d
Concentration (nM)
PS89 probe [nM]
50
250
50
50
BAP31 protein [nM]
-
-
50
200

S7

a

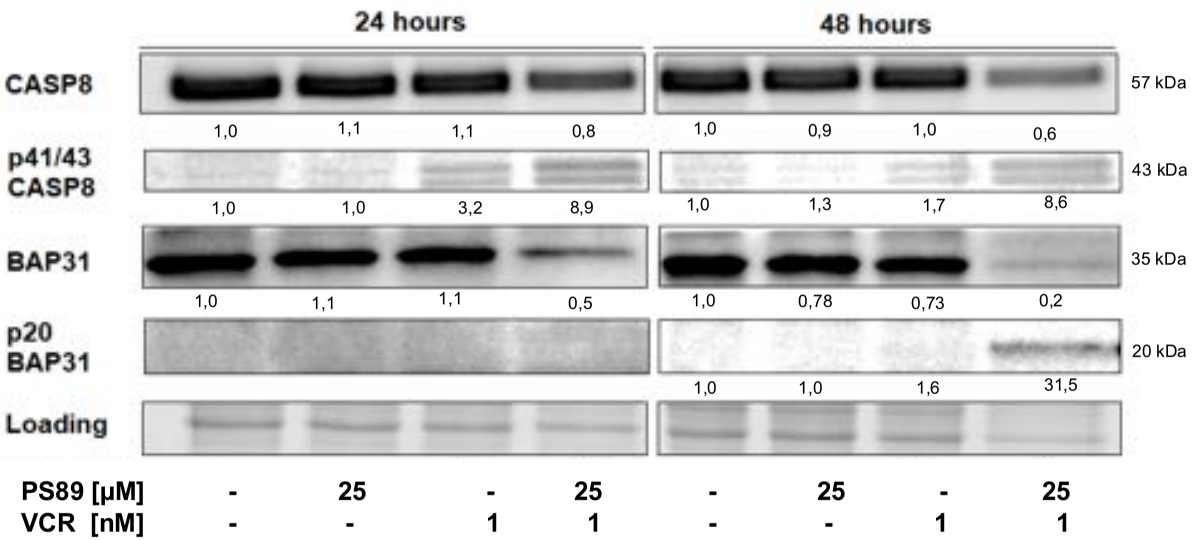
24 hours
48 hours
CASP8
57 kDa
1,0 1,1 1,1 0,8
1,0 0,9 1,0 0,6
p41/43 CASP8
43 kDa
1,0 1,0 3,2 8,9
1,0 1,3 1,7 8,6
BAP31
35 kDa
1,0 1,1 1,1 0,5
1,0 0,78 0,73 0,2
p20 BAP31
20 kDa
1,0 1,0 1,6 31,5
Loading
PS89 [µM] - 25 - 25 - 25 - 25
VCR [nM] - - 1 1 - - 1 1

b

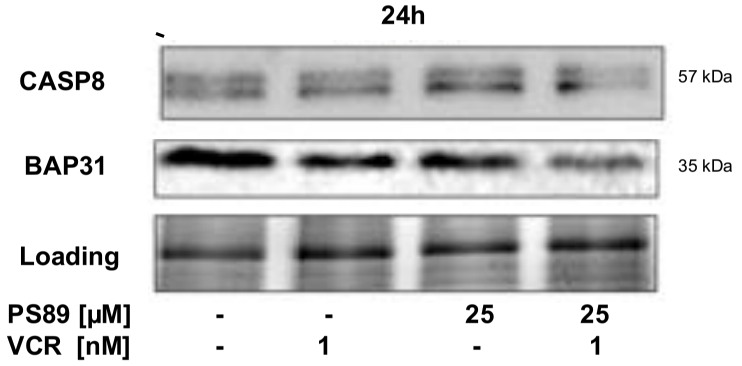
24h
CASP8
57 kDa
BAP31
35 kDa
Loading
PS89 [µM] - - 25 25
VCR [nM] - 1 - 1

S8

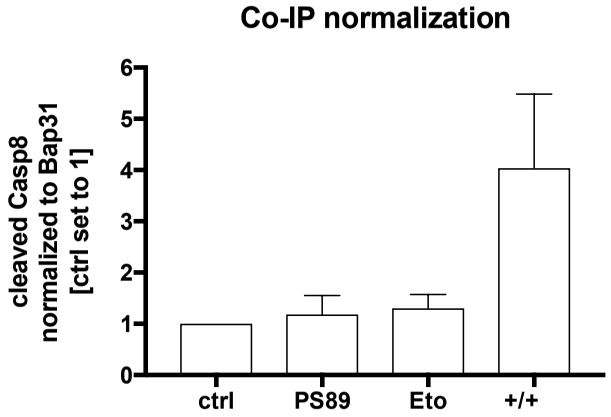
Co-IP normalization
cleaved Casp8
normalized to Bap31
[ctrl set to 1]
0
1
2
3
4
5
6
ctrl
PS89
Eto
+/+

S9

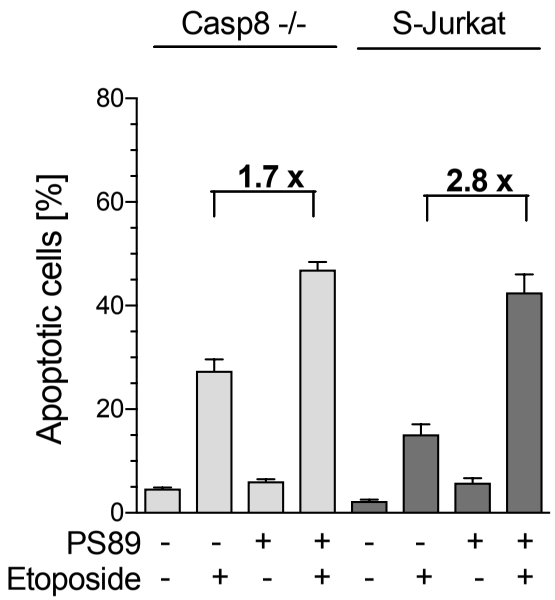
Casp8 -/-
S-Jurkat
Apoptotic cells [%]
0
20
40
60
80
1.7 x
2.8 x
PS89 - - + + - - + +
Etoposide - + - + - + - +

S10

a

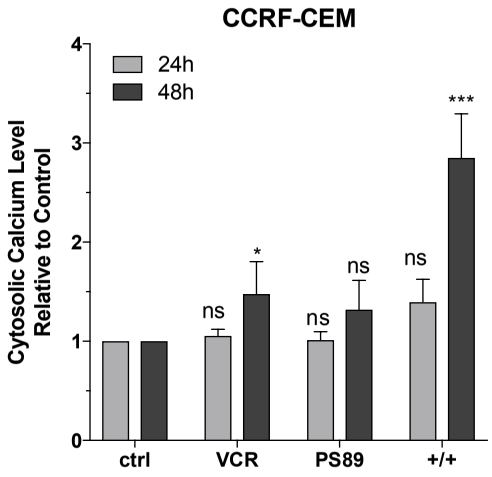
CCRF-CEM
24h
48h
Cytosolic Calcium Level
Relative to Control
0
1
2
3
4
ns
*
ns
ns
ns
***
ctrl
VCR
PS89
+/+

b

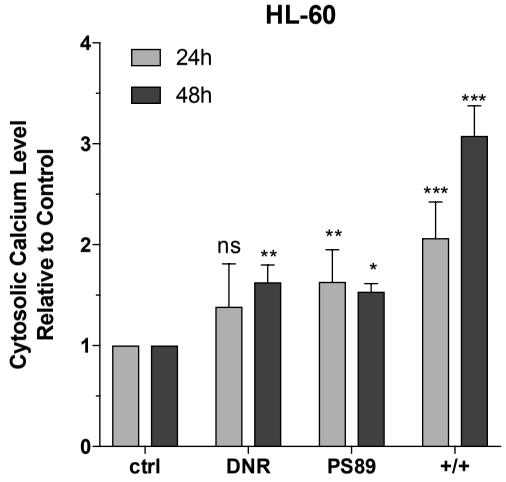
HL-60
24h
48h
Cytosolic Calcium Level
Relative to Control
0
1
2
3
4
ns
**
**
*
***
***
ctrl
DNR
PS89
+/+

c

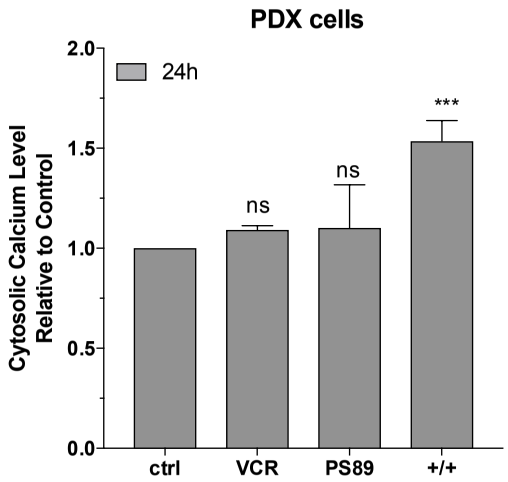
PDX cells
24h
Cytosolic Calcium Level
Relative to Control
0.0
0.5
1.0
1.5
2.0
ns
ns
***
ctrl
VCR
PS89
+/+

S11

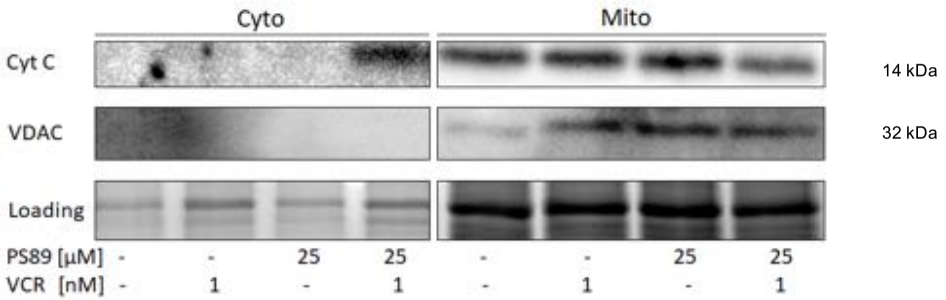
Cyto
Mito
Cyt C
VDAC
Loading
14 kDa
32 kDa
PS89 [µM] - - 25 25 - - 25 25
VCR [nM] - 1 - 1 - 1 - 1

S12

a

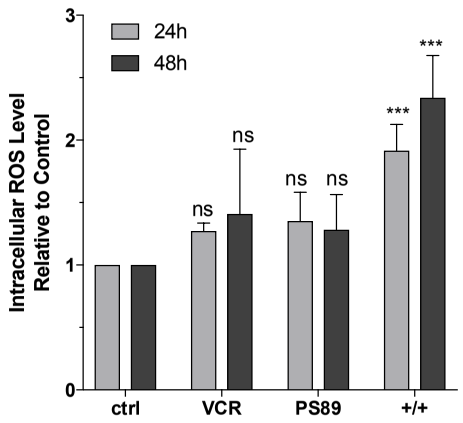
CCRF-CEM
24h
48h
Intracellular ROS Level
Relative to Control
ns
ns
ns
ns
***
***
ctrl
VCR
PS89
+/+

b

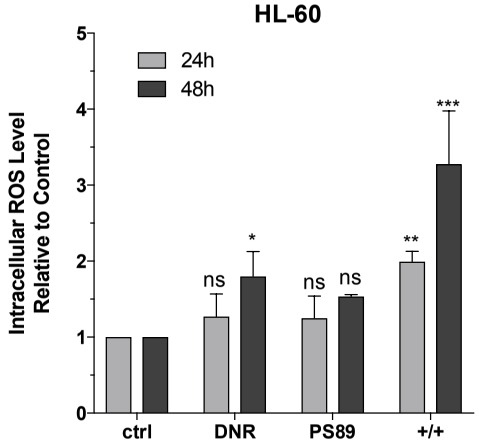
HL-60
24h
48h
Intracellular ROS Level
Relative to Control
ns
*
ns
ns
**
***
ctrl
DNR
PS89
+/+

Supplementary tables

Table S1

a

Bliss values (> 1 indicates synergism)	
0,1μM ETO + PS89	1,10
0,25μM ETO + PS89	1,22
0,5μM ETO + PS89	1,65
1μM ETO + PS89	1,72
1,5μM ETO + PS89	1,38
2μM ETO + PS89	1,18
5μM ETO + PS89	1,00
10 μM ETO + PS89	1,03

b

Bliss values (> 1 indicates synergism)	HL60	CCRF-CEM	VCR-CEM
DNR/VCR+PS89	1,98	2,73	5,96

c

p-values (Ordinary one-way ANOVA)	PBMC	ALL-168	ALL-230
25μM PS89	0,07	0,08	0,11
5nM VCR	0,79	0,06	0,05
25μM PS89+5nM VCR	0,07	0,002	0,002

d

p-values (Ordinary one-way ANOVA)	PBMC	AML-372	AML-393	AML-491	CD34+
25μM PS89	0,81	0,73	>0,99	>0,99	0,97
5nM DNR	0,67	0,82	>0,99	0,95	-
25μM PS89+5nM DNR	0,39	0,18	0,95	0,39	-
20nM DNR	0,11	0,02	0,08	<0,001	0,97
25μM PS89+20nM DNR	0,003	<0,001	0,02	<0,001	0,37

e

Brown-Forsythe test	CD34+ cells
F (DFn, DFd)	0,7336 (2,6)
p-value	0,5188
p-value summary	ns
Are SDs significantly different (p< 0,05)?	No

Table S2

Sample	Type	Subtype	Disease Stage	Sex	Age	Cytogenetics	NPM1	FLT3	BCR-ABL	MLL
ALL-168	ALL	preB ALL	initial diagnosis	female	5	46, XX, der(19)t(1;19)(q23;q13),inc			neg.	neg.
ALL-230	ALL	T ALL	initial diagnosis	male	4	46, XY, t(11;14);(p32;q11)			neg.	neg.
AML-372	AML	M0	relapse	male	42	complex, including -17	wt	wt		neg.
AML-393	AML	M4	relapse	female	47	46,XX,ins(10;11)(p12;q23q23)	wt	wt		MLL-AF10
AML-491	AML		relapse	female	53	46,XX,del(7)(q2?1)	wt	wt		neg.

Table S3

Gene names	Protein names	Mol. weight [kDa]	Probe / DMSO				Probe / PSB				Overall Score
			log2 enrichment		-log10 p-value		log2 enrichment		-log10 p-value		
			enrichment	Rank	enrichment	Rank	enrichment	Rank	enrichment	Rank	
C21orf33	ES1 protein homolog, mitochondrial	25.84	4.767	3	4.662	14	4.642	1	4.318	1	3.5
TMX1	Thioredoxin-related transmembrane protein 1	31.791	3.417	9	6.568	2	1.758	6	3.141	3	4.8
BCAP31	B-cell receptor-associated protein 31	27.991	3.725	6	5.819	4	1.543	7	2.345	6	6.0
SLC29A1	Equilibrative nucleoside transporter 1	50.219	4.584	4	4.770	13	2.130	3	2.049	7	6.2
P4HB	Protein disulfide-isomerase	57.116	5.131	1	6.927	1	1.289	10	1.956	10	7.0
EPHX2	Bifunctional epoxide hydrolase 2	62.915	3.419	8	3.416	30	3.893	2	3.315	2	7.7
PDIA6	Protein disulfide-isomerase A6	47.837	3.409	10	6.669	15	1.096	15	2.731	4	10.5
HSD17B12	Very-long-chain 3-oxoacyl-CoA reductase	34.324	2.893	16	4.242	19	1.516	8	1.999	9	11.5
SOAT1	Sterol O-acyltransferase 1	64.734	2.832	15	3.930	23	1.982	5	1.868	12	12.0
HM13	Minor histocompatibility antigen H13	36.813	4.037	5	4.637	12	1.012	17	1.637	17	14.2
CYP51A1	Lanosterol 14-alpha demethylase	58.805	2.502	18	3.158	35	2.018	4	1.668	15	15.2
PDIA4	Protein disulfide-isomerase A4	72.932	3.247	12	5.485	6	0.946	23	1.668	14	15.2
PDIA3	Protein disulfide-isomerase A3	56.782	3.464	7	6.369	3	0.830	26	1.660	16	15.7
TMEM33	Thioredoxin domain-containing protein 5	40.369	2.828	17	4.840	11	1.217	14	1.553	20	16.0
TMEM214	Transmembrane protein 214	77.15	2.315	21	4.007	22	0.916	24	2.683	5	16.8
TMEM312	Thioredoxin domain-containing protein 12	19.206	2.982	14	4.372	16	1.217	13	1.096	25	17.7
CYB5B	Cytochrome b5 type B	14.846	2.357	20	3.202	33	1.308	9	1.113	24	19.8
HMOX2	Heme oxygenase 2	36.032	3.322	11	4.212	20	0.966	21	1.093	26	20.8
KTL3	Kitaelin-3	60.541	1.757	38	5.427	8	0.803	33	1.891	8	21.0
ATP2A2	Sarcoplasmic/endoplasmic reticulum calcium ATPase 2	109.73	2.994	29	4.398	16	0.900	25	1.630	16	22.2
SPCS2	Signal peptidase complex subunit 2	17.027	2.060	30	2.835	40	1.277	11	1.469	21	22.3
VAT1	Synaptic vesicle membrane protein VAT-1 homolog	41.92	4.635	2	5.195	8	0.799	28	0.674	36	23.0
HCCS	Cytochrome c-type heme lyase	36.601	2.256	24	5.015	10	0.959	22	0.888	31	23.3
HADHA	Trifunctional enzyme subunit alpha, mitochondrial	82.999	1.803	36	4.103	21	0.760	29	1.755	13	23.5
SQLE	Squalene monooxygenase	53.067	2.996	28	3.425	29	0.976	20	1.447	22	23.5
TMPO	Lamina-associated polypeptide 2, isoforms beta/gamma	50.67	1.819	35	3.183	34	0.882	18	1.671	18	23.8
DHCR7	7-dehydrocholesterol reductase	54.469	1.801	42	4.356	17	0.960	19	1.136	23	23.8
PARK7	Protein deglycase DJ-1	19.891	2.125	26	2.823	41	1.282	12	0.982	28	24.5
ENDOD1	Endonuclease domain-containing 1 protein	55.019	1.998	32	3.019	37	0.728	30	1.908	11	25.2
CLPTM1L	Cleft lip and palate transmembrane protein 1-like protein	58.355	2.466	19	3.692	25	0.713	31	1.026	27	26.7
VDAC2	Voltage-dependent anion-selective channel protein 2	31.566	2.261	23	5.264	7	0.415	37	0.892	30	27.3
PRKCSH	Glucosidase 2 subunit beta	60.192	1.815	41	3.063	36	1.060	16	0.685	32	28.8
DNPEP1	Thioredoxin reductase 1, cytoplasmic	60.078	2.092	27	3.288	31	0.592	34	0.901	29	30.7
VDAC3	Voltage-dependent anion-selective channel protein 3	30.656	2.300	22	5.173	9	0.266	40	0.557	37	30.8
ALDH9A2	Fatty aldehyde dehydrogenase	44.648	2.986	13	3.772	24	0.435	36	0.164	41	31.8
SACM1L	Phosphatidylinositide phosphatase SAC1	66.966	1.850	40	3.446	27	0.800	32	0.852	34	33.2
LRRC59	Leucine-rich repeat-containing protein 59	34.93	2.049	31	3.437	28	0.531	35	0.727	35	33.2
COMT	Catechol O-methyltransferase	24.449	1.987	33	2.588	42	0.803	27	0.455	38	34.2
FKBP8	Peptidyl-prolyl cis-trans isomerase FKBP8	44.591	1.764	39	3.279	32	0.330	38	0.671	33	35.5
CANX	Calnexin	67.567	1.789	37	3.097	26	0.278	41	0.308	40	37.5
DCXR1	DCIA domain-containing protein 1	27.626	1.871	34	2.993	39	0.327	39	0.357	39	38.2
NT5DC1	5-nucleotidase domain-containing protein 1	51.844	2.129	25	2.998	38	0.120	42	0.086	42	38.5

Table S4

	Bliss values (> 1 indicates synergism)
0,5μM ABT-199 + PS89	1,21
1μM ABT-199 + PS89	1,53
2μM ABT-199 + PS89	1,54
3μM ABT-199 + PS89	1,92
5μM ABT-199 + PS89	1,53
10μM ABT-199 + PS89	1,48
25μM ABT-199 + PS89	1,06
50 μM ABT-199 + PS89	1,00
100 μM ABT-199 + PS89	0,94